The Astrophysical Journal, 623:650–665, 2005 April 20

FORMATION OF GLOBULAR CLUSTERS IN HIERARCHICAL COSMOLOGY

Andrey V. Kravtsov
Department of Astronomy and Astrophysics and Kavli Institute for Cosmological Physics, Enrico Fermi Institute, University of Chicago, 5640 South Ellis Avenue, Chicago, IL 60637; andrey@oddjob.uchicago.edu

and

Oleg Y. Gnedin
Space Telescope Science Institute, 3700 San Martin Drive, Baltimore, MD 21218; ognedin@stsci.edu
Received 2003 May 12; accepted 2004 December 25

ABSTRACT

We study the formation of globular clusters in a Milky Way–size galaxy using a high-resolution cosmological simulation. The clusters in our model form in the strongly baryon-dominated cores of supergiant molecular clouds in the gaseous disks of high-redshift galaxies. The properties of clusters are estimated using a physically motivated subgrid model of the isothermal cloud collapse. The first clusters in the simulation form at $z \approx 12$, while we conjecture that the best conditions for globular cluster formation appear to be at $z \sim 3$–5. Most clusters form in the progenitor galaxies of the virial mass $M_h > 10^9\ M_\odot$, and the total mass of the cluster population is strongly correlated with the mass of its host galaxy: $M_{\rm GC} = 3 \times 10^6\ M_\odot (M_h/10^{11}\ M_\odot)^{1.1}$. This corresponds to a fraction $\sim 2 \times 10^{-4}$ of the galactic baryons being in the form of globular clusters. In addition, the mass of the globular cluster population and the maximum cluster mass in a given region strongly correlate with the local average star formation rate. We find that the mass, size, and metallicity distributions of the globular cluster population identified in the simulation are remarkably similar to the corresponding distributions of the Milky Way globular clusters. We find no clear mass-metallicity or age-metallicity correlations for the old clusters. The zero-age mass function of globular clusters can be approximated by a power law $dN/dM \propto M^{-\alpha}$ with $\alpha \approx 2$, in agreement with the mass function of young stellar clusters in starbursting galaxies. We discuss in detail the origin and universality of the globular cluster mass function. Our results indicate that globular clusters with properties similar to those of observed clusters can form naturally within dense gaseous disks at $z \gtrsim 3$ in the concordance ΛCDM cosmology.

Subject headings: cosmology: theory — galaxies: formation — galaxies: star clusters — globular clusters: general — methods: numerical

1. INTRODUCTION

More than 70 years ago in a monograph entitled "Star Clusters" Harlow Shapley wrote, "It is encouraging to see how fragile and futile are the majority of astronomical theories and speculations . . . for the futility of speculations emphasizes the importance and durability of observations and indicates the steady progress of the science" (Shapley 1930, p. 193). These words are particularly true for the models of globular cluster (GC) formation. Extensive observational surveys of GC systems in the Milky Way and other galaxies have been compiled during the past two decades (e.g., Harris 2001). At the same time, despite a wide variety of proposed models, a self-consistent scenario of GC formation is yet to be constructed.

The existing models can be classified into four broad categories. In the primary models globular clusters are envisioned to have formed soon after recombination, with masses determined by the cosmological Jeans mass (Peebles & Dicke 1968; Peebles 1984). In the secondary models, globular clusters are assumed to appear during the early stages of galaxy formation. For instance, Fall & Rees (1985) pointed out that thermal instability in hot gaseous halos of young galaxies can naturally lead to the condensation of GC-size clouds. Several other trigger mechanisms operating during galaxy formation, such as the shock compression and collisions of primordial molecular clouds, were also explored (Gunn 1980; Burkert et al. 1992; Murray & Lin 1992; Larson 1996; Harris & Pudritz 1994; Cen 2001).

Models of the third class correspond to the relatively recent stages of galaxy formation. Schweizer (1987) and Ashman & Zepf (1992), for example, proposed a model of GC formation in the gas-rich mergers of disk galaxies. The mergers perturb, compress, and shock the interstellar medium (ISM), which creates the very high pressure regions conducive to GC formation. Accordingly, this model predicted that young clusters should be present in merging and interacting galaxies. These predictions were successfully confirmed by *Hubble Space Telescope* (*HST*) observations (Whitmore & Schweizer 1995; Holtzman et al. 1996; Whitmore et al. 1999; Zepf et al. 1999).

The division between the second and third classes of models is somewhat blurred. In the current hierarchical structure formation paradigm, galaxy formation is a continuous process of merging and accretion. The fourth, most recent class of models thus incorporates the elements of all previous classes within the hierarchical framework (Côté et al. 2000, 2002; Beasley et al. 2002; Gnedin 2003). Globular clusters in these models are assumed to form in young disks that undergo frequent mergers. At this point, the models are largely phenomenological and characterize the cluster formation using somewhat ad hoc recipes, limiting their predictive power. Nevertheless, they have been fairly successful in reproducing many properties of the observed GC populations. The comparisons of various models to observations can be found in Harris (2001) and Gnedin et al. (2001).

The main obstacle to building a realistic and self-consistent physical model of globular cluster formation has always been the uncertainty in the initial conditions. In fact, all of the models mentioned above would produce star clusters in environments where the conditions agree with the model assumptions. Another unknown is the connection between globular clusters and galaxies.

On the one hand, the largest globular clusters have masses comparable to those of dwarf spheroidal galaxies ($\sim 10^7\,M_\odot$). On the other, globular clusters do not seem to have extended dark matter (DM) halos (e.g., Moore 1996) and in that respect differ fundamentally from galaxies. There is also significant disparity between the densities, velocity dispersions, and structural parameters of dwarf galaxies and globular clusters (Kormendy 1985). In order to understand these differences, we need a self-consistent model that ties the formation of globular clusters to the realistic formation and evolution of their parent galaxies.

The theory of hierarchical galaxy formation has matured in the last decade, motivated by the theory of inflation, guided by observations, and aided by elaborate numerical simulations. In hierarchical models, galaxies form via gravitational instability from small-amplitude initial Gaussian fluctuations with well-defined statistical properties. Recently, this scenario has been spectacularly confirmed by the cosmic microwave background (CMB) anisotropy measurements and other cosmological probes (e.g., Spergel et al. 2003). The spatially flat cosmological model dominated by the dark energy and cold dark matter (ΛCDM) favored by observations provides a solid framework for the theory of GC formation.

Cosmological simulations follow the hierarchical buildup of galaxies self-consistently starting from the well-defined initial conditions. These simulations are now reaching the level of sophistication and dynamic range sufficient to study the formation and dynamics of giant molecular clouds in galactic disks. Therefore, we can address the formation of the protocluster clouds without resorting to phenomenological parameterization and directly study the details of when, where, and how globular clusters formed.

The main goal of this work is to study the formation of GC populations in the hierarchical scenario using a very high resolution cosmological simulation. Based on observational evidence, we assume that clusters form in dense isothermal cores of the supergiant molecular clouds ubiquitous in high-redshift galactic disks. In addition, we use a simple model of isothermal collapse to derive the properties of stellar clusters that would form in such cores. We then compare the derived properties of model globular clusters with those of the GC population in the Galaxy, as well as with the populations of young globular clusters in external galaxies.

Many decades ago, Harlow Shapley used the distribution of globular clusters to greatly expand and redefine the structure of our Galaxy. It is only fitting that we now apply our understanding of galaxy formation to predict and explain the properties of globular clusters.

2. NUMERICAL SIMULATIONS

2.1. *Numerical Techniques and Physical Processes*

The simulation presented in this paper was performed using the Eulerian gasdynamics plus *N*-body Adaptive Refinement Tree (ART) code. This code is based on the cell-based approach to adaptive mesh refinement developed by Khokhlov (1998). The algorithm uses a combination of multilevel particle-mesh (Kravtsov et al. 1997; Kravtsov 1999) and shock-capturing Eulerian methods (van Leer 1979; Colella & Glaz 1985) to follow the evolution of DM and gas, respectively. High dynamic range is achieved by applying adaptive mesh refinement to both the gasdynamics and gravity calculations.

Several physical processes critical to various aspects of galaxy formation are implemented in this code: star formation; metal enrichment and thermal feedback due to Type II and Type Ia supernovae (SNe II/Ia); self-consistent advection of metals; and metallicity- and density-dependent cooling and UV heating due to the cosmological ionizing background, using the cooling and heating rates tabulated in the temperature range $10^2\ \mathrm{K} < T < 10^9\ \mathrm{K}$ for a grid of densities, metallicities, and UV intensities using CLOUDY (ver. 96b4; Ferland et al. 1998). In the present simulations we set a minimum temperature of $T_{\min} = 300$ K. The cooling and heating rates take into account Compton heating/cooling of plasma, UV heating, and atomic and molecular cooling. While the detailed implementation of these processes is described elsewhere (Kravtsov 2003), below we summarize the details crucial to this study.

We use a "constant-efficiency" star formation prescription. Namely, the stars are formed with a *constant* timescale τ_* so that the star formation rate is proportional to the local gas density, $\dot{\rho}_* \propto \rho_g$. This prescription is motivated by observations of the star-forming regions (e.g., Young et al. 1996; Wong & Blitz 2002) and appears to reproduce the Schmidt-like law of star formation on kiloparsec scales (Kravtsov 2003). Star formation is allowed to take place only in the coldest and densest regions, $T < T_{\rm SF}$ and $\rho_g > \rho_{\rm SF}$, but no other criteria (like the collapse condition $\nabla \cdot \boldsymbol{v} < 0$) are imposed. We use $\tau_* = 4$ Gyr, $T_{\rm SF} = 9000$ K, and $\rho_{\rm SF} = 1.64\,M_\odot\ \mathrm{pc}^{-3}$ or the atomic hydrogen number density of $n_{\rm H} = 50\ \mathrm{cm}^{-3}$. The adopted values of $T_{\rm SF}$ and $\rho_{\rm SF}$ are quite different from the typical temperatures and densities of star-forming molecular cores: $T \lesssim 30$–50 K and $n_{\rm H} \gtrsim 10^4\ \mathrm{cm}^{-3}$. They are, however, more appropriate for the identification of star-forming regions on $\sim$100 pc scales that are resolved in the present simulation. In practice, $T_{\rm SF}$ is not relevant because most of the gas with $\rho > \rho_{\rm SF}$ is at temperatures of just a few hundred kelvins.

Each newly formed stellar particle is treated as a single-age stellar population, and its feedback on the surrounding gas is implemented accordingly. The word feedback is used here in a broad sense to include the injection of energy and heavy elements (metals) via stellar winds and supernovae, as well as the secular stellar mass loss. Specifically, we assume that the stellar initial mass function (IMF) is described by the Miller & Scalo (1979) functional form with stellar masses in the range 0.1–100 $M_\odot$. All stars with $m_* > 8\,M_\odot$ deposit 2×10^{51} ergs of thermal energy and a mass $f_Z m_*$ of heavy elements in their parent cell (no delay of cooling is introduced in these cells). The metal fraction is $f_Z = \min(0.2,\ 0.01 m_* - 0.06)$, which crudely approximates the results of Woosley & Weaver (1995). In addition, the stellar particles return a fraction of their mass and metals to the surrounding gas at a secular rate $\dot{m}_{\rm loss} = m_* C_0 (t - t_{\rm birth} + T_0)^{-1}$ with $C_0 = 0.05$ and $T_0 = 5$ Myr (Jungwiert et al. 2001). The released metals are advected along with the gas. The code also accounts for SN Ia feedback assuming a rate that slowly increases with time and broadly peaks at the population age of 1 Gyr. We assume that the fraction 5×10^{-3} of mass in stars between 3 and 8 $M_\odot$ explodes as SNe Ia over the entire population history and each SN Ia dumps 2×10^{51} ergs of thermal energy and ejects 1.3 $M_\odot$ of metals into the parent cell. For the assumed IMF, 75 SNe II (instantly) and 11 SNe Ia (over several billion years) are produced by a $10^4\,M_\odot$ stellar population.

2.2. *Simulation Parameters*

The simulation we use in our analysis follows the early ($z \gtrsim 3$) stages of evolution for a galaxy of typical mass: $\approx 10^{12}\,h^{-1}\,M_\odot$ at $z = 0$. At the analyzed epochs, the galaxy has already built up a significant portion of its final mass: $1.3 \times 10^{10}\ h^{-1}\ M_\odot$ at $z = 9$ and $2 \times 10^{11}\ h^{-1}\ M_\odot$ at $z = 4$. The total galaxy mass, M_h, is defined as the mass enclosed within the radius of the average

density equal to 340 times the mean matter density. The simulation starts from a random realization of the Gaussian density field at $z = 50$ in a periodic box of $6\,h^{-1}$ comoving Mpc with the power spectrum (Hu & Sugiyama 1996) appropriate to the flat ΛCDM model: $\Omega_0 = 1 - \Omega_\Lambda = 0.3$, $\Omega_b = 0.043$, $h = H_0/100 = 0.7$, $n_s = 1$, and $\sigma_8 = 0.9$. The parameters have their usual meaning and are consistent with recent cosmological constraints (e.g., Spergel et al. 2003).

To increase mass resolution, a low-resolution simulation was run first and a galactic-mass halo was selected. A Lagrangian region corresponding to five virial radii of the object at $z = 0$ was then identified at $z = 50$ and resampled with additional small-scale waves (Klypin et al. 2001). The total number of DM particles in the high-resolution Lagrangian region is 2.64×10^6, and each particle mass is $m_{\rm DM} = 9.18 \times 10^5\,h^{-1}\,M_\odot$. Outside the high-resolution region the matter distribution was sampled with $\approx 3 \times 10^5$ higher mass particles.

As the matter distribution evolves, the code adaptively and recursively refines the mesh in the high-density regions. Initially, a uniform 64^3 grid covered the entire computational box. The Lagrangian region, however, was always unconditionally refined to the third refinement level, corresponding to an effective grid size of 512^3. Beyond the third level, a mesh cell was tagged for refinement if its gas *or* DM mass exceeded 0.125 and 0.0625 times the mean mass expected for the average density in each component in the zeroth level (i.e., uniform grid) cell, respectively. The refinement follows the collapse of 1.2×10^6 (gas) and $3.7 \times 10^6\,h^{-1}\,M_\odot$ (DM) mass elements in a quasi-Lagrangian fashion. These masses can be loosely considered as gas mass resolution until the maximum level is reached beyond which refinements are not done. In the run we use this level is set to $l_{\rm max} = 9$ and is reached by $z \approx 10$. Beyond this, the notion of mass resolution for gas is not well defined because gas is represented as a continuous medium on an Eulerian mesh. Once the maximum refinement level is reached, the mass per cell then is no longer constant but reflects the local gas density. For example, cells of the ninth level have gas densities spanning the range of more than 6 orders of magnitude as the ISM is multiphase with tenuous hot gas and very dense cold gas occupying different regions (see, e.g., Fig. 9 below).

The spatial resolution of the simulation is thus time dependent. As the density increases, additional refinement levels are added to keep the mass per cell approximately constant. The maximum allowed refinement level $l_{\rm max}$ was set to 9, and this level was reached at $z \approx 10$. In the simulation we present, the physical size of the maximum refinement cell is $\sim$28, 20, 26, 37, and $45\,h^{-1}$ pc at $z = 12$, 9, 6, 4, and 3, respectively. Thus, the change over the analyzed range of epochs is not very large. A total of $\approx 1.1 \times 10^7$ mesh cells were used at $z = 4$ with $\approx 2.5 \times 10^5$ of them at refinement levels of 8 and 9. The high-density cold star-forming disks within DM halos were refined to $l_{\rm max} = 9$. The physical size of mesh cells was $\Delta x_l = 26.16[10/(1+z)]2^{9-l}$ pc, where l is the cell's level of refinement. Each refinement level was integrated with its own time step $\Delta t_l = \Delta t_0 2^{-l} \approx 2^{9-l} \times 2 \times 10^4$ yr, where $\Delta t_0 \lesssim 10^7$ yr is the global time step on the zeroth level set using the Courant-Friedrichs-Levy condition.

2.3. *Identification of the Globular Cluster Formation Sites*

Although the resolution achieved in the simulation is very high in the disk region, it is still insufficient to resolve the formation of stellar clusters. The resolution, however, is sufficient to identify the potential sites for GC formation. The cores of giant molecular clouds in high-redshift galaxies are the natural candidates (Harris & Pudritz 1994; McLaughlin & Pudritz 1996) for such sites. Numerical simulations of Nakasato et al. (2000) show that globular clusters with realistic masses and sizes can indeed form in such cores. We therefore adopt this picture and identify the cores of dense gaseous clouds in simulated disks as the sites of GC formation.

We identify giant molecular clouds using the following algorithm. All mesh cells with gas densities greater than a certain threshold density, $\rho_{\rm mc}$, are selected and sorted into a list of increasing density. The highest density cell and all of its immediate neighbors are then included in the first cloud. This cell is labeled as the core cell of the cloud. The next highest density cell in the list is then considered. If it happens to be already included in the first cloud, all of its immediate neighbor cells are then also included in the first cloud. If, on the other hand, the cell is not part of a cloud yet, it is assigned to a new cloud and is labeled as its core. The procedure repeats until the list of cells is exhausted. The algorithm is thus somewhat similar, but not equivalent, to the well-known friends-of-friends clustering algorithm. The current implementation will break a region into separate clouds for each density peak rather than combining several peaks into the same cloud.

We explored several values of the threshold density $\rho_{\rm mc} = 1$–$50\ M_\odot\ {\rm pc}^{-3}$. Although the cloud masses grow and ever smaller clouds are included in the catalog as the threshold is decreased, in the mass range relevant for the GC identification the same cores are recovered for all $\rho_{\rm mc}$. For our analysis below we choose the cloud catalog with the fiducial value $\rho_{\rm mc} = 1\ M_\odot\ {\rm pc}^{-3}$. This corresponds to the gas number density $\approx 40\ {\rm cm}^{-3}$ and pressure $\gtrsim 10^4\ {\rm K\ cm}^{-3}$. Note that at these densities the gas temperature is at the lowest value allowed in the simulation: $T_{\rm min} = 300$ K.

2.4. *The Subgrid Model*

In order to derive the properties of star clusters forming in molecular cloud cores, we complement the simulations with a physical description of the gas distribution on a subgrid level. Observations of star-forming regions in the solar neighborhood (e.g., Elmegreen 2002) show that clustered star formation proceeds inevitably when the cores of molecular clouds reach a critical density $\gtrsim 10^5\ {\rm cm}^{-3}$. Formation of young massive clusters is also accompanied by high external pressure, $P > 10^7$ K cm^{-3}. Within such cores, star clusters form with a locally high efficiency (Geyer & Burkert 2001; Kroupa et al. 2001; Kroupa & Boily 2002),

$$\epsilon \equiv \frac{M_*}{M_g} \gtrsim 0.5, \qquad (1)$$

which is required in order to produce gravitationally bound clusters. On the theoretical side, analytical models and numerical simulations also indicate that dense bound clusters can form quickly and efficiently in the cores of giant molecular clouds of moderate metallicity (e.g., Harris & Pudritz 1994; McLaughlin & Pudritz 1996; Nakasato et al. 2000). In the models of molecular clouds including thermal support, turbulence, and magnetic fields star formation proceeds rapidly, on one or two dynamical times (Pringle 1989; Ostriker et al. 2001; Bate et al. 2003). Based on these observational and theoretical results, we implement the following phenomenological subgrid model.

At high densities in the central cells of the identified gas clouds the cooling time is much shorter than the dynamical time; therefore, the cells must be isothermal. Indeed, the resolved structure of the molecular clouds in the simulation has an isothermal profile, $\rho_g \propto r^{-2}$. We thus extrapolate this profile inside the

central unresolved cell. (Such isothermal structure is also predicted by the simulations of the collapse of cloud cores by Nakasato et al. [2000].) What we measure in the simulation is the cell-averaged gas density, $\rho_{\rm cell} \equiv \rho_{\rm av}(<R_{\rm cell})$, where $R_{\rm cell}$ is the cell radius (a half of the cell dimension). For an isothermal profile the average density within $R_{\rm cell}$ is $\rho_{\rm av}(<R_{\rm cell}) = 3\rho_g(R_{\rm cell})$. We can thus derive the inner density profile as

$$\rho_g(r < R_{\rm cell}) = \frac{1}{3}\rho_{\rm cell}\left(\frac{r}{R_{\rm cell}}\right)^{-2}. \quad (2)$$

We assume that a single cluster forms within the cloud core on a dynamical (free-fall) time at the densities higher than the critical, $\rho_{\rm CSF}$. To distinguish from the field star formation denoted by the subscript "SF" in § 2.1, here the subscript "CSF" stands for "clustered star formation." By choosing a density threshold, we postulate that only a high-density tail of the gas distribution produces compact massive clusters, whereas the rest (and most) of the gas participates in the formation of field stars or open clusters. This scenario is quite natural. High gas densities are required to match the observed stellar densities, which are highest in globular clusters. A single value of the density threshold, of course, is not sufficient to describe complex physics of molecular clouds, but it can be very useful in defining the properties of the clusters, as we demonstrate below.

The radius of the molecular core going into clustered star formation $R_{\rm CSF}$ is determined by the condition $\rho_g(R_{\rm CSF}) = \rho_{\rm CSF}$. All gas within $R_{\rm CSF}$ is converted into stars with the efficiency ϵ:

$$M = \epsilon M_g(R_{\rm CSF}) = \epsilon 4\pi\rho_{\rm CSF}R_{\rm CSF}^3. \quad (3)$$

The fraction $1 - \epsilon$ of the core mass remaining in the gas phase will be expelled from that region, following the formation of UV-bright O and B stars. As a result of the gradual loss of the remaining gas, the star cluster expands almost adiabatically (e.g., Geyer & Burkert 2001; Boily & Kroupa 2003) such that its final size is

$$R = \frac{1}{\epsilon}R_{\rm CSF} = \frac{1}{\epsilon}R_{\rm cell}\left(\frac{\rho_{\rm cell}}{3\rho_{\rm CSF}}\right)^{1/2}. \quad (4)$$

The resulting average density of the clusters is

$$\rho \equiv \frac{M}{(4\pi/3)R^3} = \epsilon^4\frac{M_g(R_{\rm CSF})}{(4\pi/3)R_{\rm CSF}^3} = 3\epsilon^4\rho_{\rm CSF}. \quad (5)$$

We use the fiducial values $\epsilon = 0.6$ and $\rho_{\rm CSF} = 10^4\ M_\odot\ {\rm pc}^{-3}$, which gives $\rho \approx 4\times10^3\ M_\odot\ {\rm pc}^{-3}$. It is close to the median density at the half-mass radius for the Milky Way GCs, which is $3\times10^3\ M_\odot\ {\rm pc}^{-3}$.

Although the expressions for the mass and size of star clusters are linked to the resolution-dependent cell properties ($\rho_{\rm cell}, R_{\rm cell}$), the parameters of individual clusters are almost insensitive to changes in the resolution. This is because the cores of dense molecular clouds in which GCs form are isothermal. Thus, when the cell size $R_{\rm cell}$ changes, the cell density adjusts as $\rho_{\rm cell} \propto R_{\rm cell}^{-2}$, leaving the radius $R_{\rm CSF}$ and the cluster radius R and mass M unchanged (see eqs. [3] and [4]). This is indeed what we find in the test presented below in § 5. When we repeat the analysis decreasing the level of refinement ($l_{\rm max} - 1$), the masses of individual clusters do not change significantly.

In the following we present the properties of the model clusters based on the density criterion. For completeness, in § 6.3 we discuss and evaluate alternative subgrid models and show that our model works best in reproducing the observed properties of clusters.

Note that the mass function of globular clusters at birth will be significantly modified by the effects of dynamical evolution. As we discuss in § 6.1, low-mass and low-density clusters are preferentially dissolved by the combined effects of two-body relaxation, tidal shocking, dynamical friction, and stellar evolution. High-mass clusters ($M \gtrsim 10^5\ M_\odot$), on the other hand, preserve their mass function and trace the initial distribution.

3. RESULTS

We analyze the simulation outputs at 12 epochs between redshifts $z = 11.8$ and 3.35, identifying the cores of the giant molecular clouds and computing properties of the model GCs, as described in §§ 2.3 and 2.4. The time intervals between the outputs are in the range ~100–300 Myr. Because of limited computational resources, the simulation was run only until $z = 3.3$.

3.1. *Spatial Distribution of Globular Clusters at High Redshifts*

Before discussing the detailed properties of model clusters, we first consider their spatial distribution. Figure 1 shows the density and temperature maps, as well as the velocity field of gas, in the region of the most massive disk at $z = 4$. The cooling of the gas in these regions is very fast, and the cold gas always settles in a thin disk. Frequent interactions drive strong spiral density waves in the gaseous disks, which fragment into separate molecular clouds. GCs identified within those clouds are represented by circles in the density map. The figure shows that clusters in our model form in the dense cold regions, generally tracing the spiral arms of the galaxy. The morphology of the distribution is very similar to that of young stellar clusters observed in starburst galaxies (e.g., Whitmore & Schweizer 1995; Zhang et al. 2001).

At this epoch the parent halo of the disk experiences frequent mergers and vigorous accretion of fresh gas. The two cold knots outside the spiral arms, for instance, are the small-mass satellite galaxies in the process of merging with the central halo. The dense gas in these satellites could have been compressed by the external pressure and shocks accompanying their collision with the disk. The galaxy as a whole exhibits frequent bursts of star formation associated with minor and major mergers. These mergers destroy the short-lived disks and scatter away young stars and star clusters in a spheroidal halo. The cold gas, on the other hand, always falls back to form a new thin disk.

Figure 2 shows the spatial distribution of model GCs within the large-scale structure formed in our simulation at $z = 7$ and 4. The distribution of DM is typical of hierarchical models. Visually, it is dominated by prominent filaments on large scales and hundreds of dense DM halos tracing these filaments on small scales. The figure shows that parent halos of GCs are tracing the skeleton of the large-scale structure. They concentrate in the densest regions of the filaments close to the central massive object. In other words, the distribution of halos containing clusters is *highly biased* with respect to the overall distribution of matter. This bias is especially pronounced at $z = 7$. The highly clustered distribution of halos at the early epochs is a generic feature of the hierarchical models, in which objects of galactic mass correspond to the relatively high peaks in the initial Gaussian density field. This property can be extremely important for explaining the present distribution of GCs in the halo of the Milky Way. The high spatial bias of globular clusters at early epochs would result in the more concentrated radial distribution of GCs compared to the DM today (West 1993) and

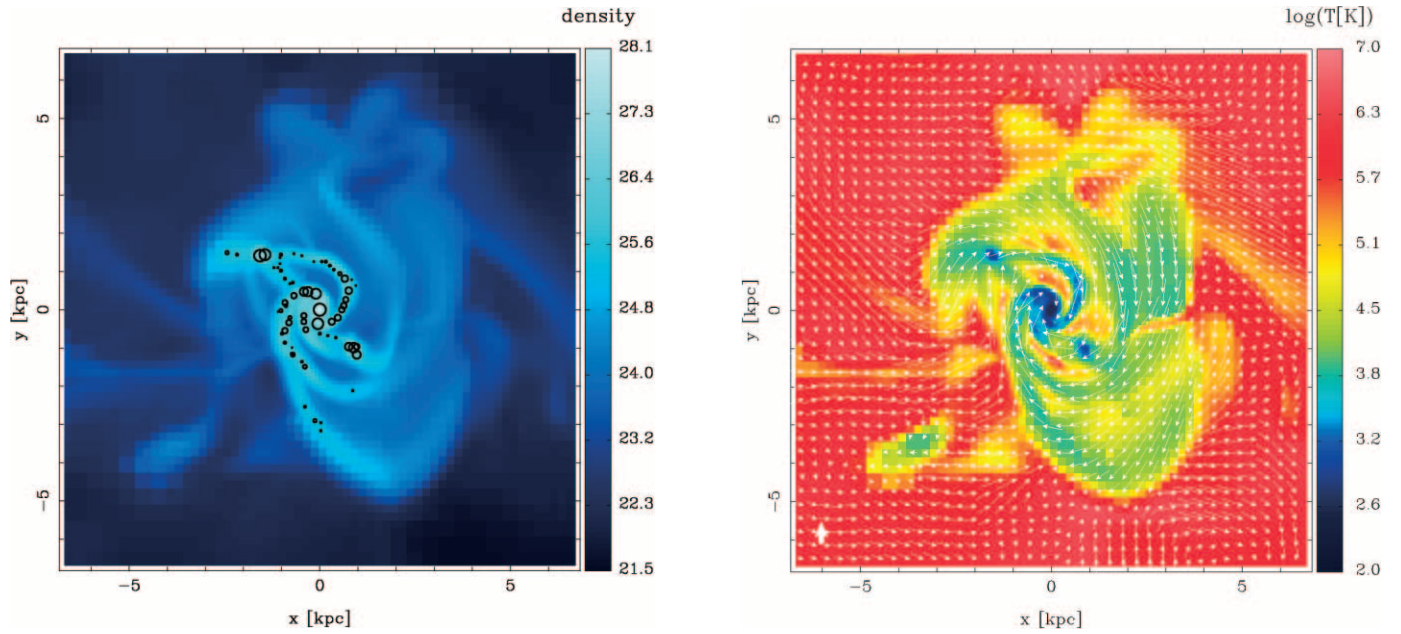

FIG. 1.—Gas density (*left*) and temperature (*right*) in the most massive disk at $z = 4$. The projected density is in cm^{-2}, while the density-weighted average temperature is in kelvins. The vectors in the right panel show gas velocities; the thick vertical vector in the lower left corner of the panel corresponds to 200 km s^{-1}. The density and temperature are projected over a 3.5 kpc slice centered on the cell of the maximum gas density (the center of the plot). The figure shows a nearly face-on disk with prominent spiral arms in the process of very active accretion and merging. In our model the globular clusters form in the densest regions of the disk corresponding to the darkest knots in the temperature map. The globular clusters identified in the disk at this epoch are shown by circles in the left panel. The radius of the circles corresponds to the mass of each cluster.

in the preferential location of higher metallicity clusters toward the center, in agreement with observations (Djorgovski & Meylan 1994; van den Bergh 2003).

Note that although the high-redshift GCs form in dense gaseous disks, the subsequent accretion of their parent galaxies along filaments will lead to tidal stripping and disruption. For example, analysis of the evolution of Milky Way–size progenitors (Kravtsov et al. 2004) shows that most of the dwarf-size systems that are located within $\lesssim 3$ virial radii from the progenitor at $z > 4$ accrete early and are disrupted before the present-day epoch. This includes most of the objects hosting GCs in Figure 2. The disrupted systems form a diffuse DM halo and contribute to the stellar halo of the host (Bullock et al. 2001). Their clusters would share the fate of the stripped stars and should therefore have spatial distribution at $z = 0$ similar to the stellar halo stars. Direct observational evidence of disruption is provided by the extended tidal tails around GCs (e.g., Odenkirchen et al. 2003; Sohn et al. 2003), around dwarf satellite galaxies (Freeman & Bland-Hawthorn 2002 and references therein), and the possible association between the two (Lynden-Bell & Lynden-Bell 1995). We will investigate the dynamical evolution and the present-day spatial distribution of the GC population in our model in a future study.

3.2. *Molecular Clouds in the Dense High-Redshift Disks*

The globular clusters in our model form in the high-density cores of giant molecular clouds of the high-redshift galaxies (Fig. 1). It is therefore important to consider the properties of the molecular clouds in connection with the properties of GCs and host galaxies. Figure 3 shows the evolution of density and metallicity in the central cell of the most massive disk shown in Figure 1. Although this cell has the highest gas density and is located at the bottom of the potential well, the overall evolution is common for all cells. The gas density exhibits several prominent peaks associated with the fast episodes of accretion. Cold metal-poor gas is delivered to the center of the disk by both merging of smaller galaxies and direct accretion of gas along a filament that reaches inside the disk region. The rapid increase of the density and pressure in the cell during the accretion events can trigger the collapse of the molecular cloud. The gas density saturates at lower redshifts ($z \lesssim 5$) as the accretion on the center of the disk slows down.

The bottom panel of Figure 3 shows the evolution of metallicity due to the SN ejecta (the contribution of SNe Ia to the metallicity is negligible at these epochs). The metallicity quickly increases to about 10% of solar and then evolves slowly. Note that the events of accretion of the fresh low-metallicity gas may lower the mean metallicity, even in the very central region. If a series of globular clusters forms between $z = 8$ and 4 in this region, the younger ones are not necessarily more metal-rich than the older ones. The age difference of these clusters would, however, be less than 2 Gyr.

Overall, the galaxies in the simulation exhibit a well-defined correlation between the stellar mass and the average metallicity of stars, $Z \propto M_*^{0.5}$, similar to the correlation observed in nearby dwarf galaxies (Dekel & Woo 2003). There is also a significant spread in gas metallicity even within a single object, which indicates that mixing of metals is rather inefficient. The wide range of gas metallicity in star-forming regions eliminates any clear age-metallicity correlation for high-redshift clusters. For instance, stars formed at the same epoch can have metallicities different by up to 2 orders of magnitude. This may also at least partially explain the well-known "second parameter problem" (e.g., Carney 2001).

The efficiency of GC formation, i.e., the ratio of the GC mass to the mass of the molecular, baryonic, or DM system containing it, depends on the averaging scale. Within the cores of giant molecular clouds the local efficiency is of the order unity (§ 2.4). Averaged over the whole molecular cloud, however, the efficiency is much lower because most of the molecular gas is not participating

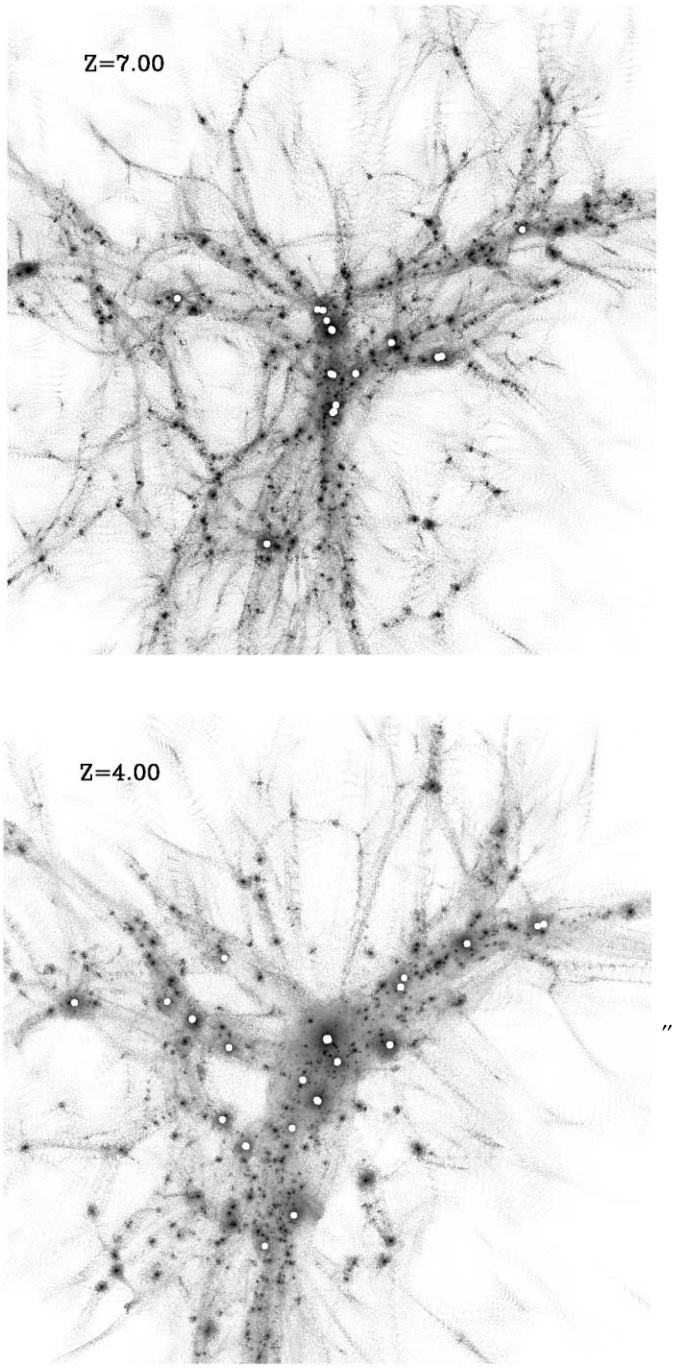

FIG. 2.—Identified globular clusters within the global distribution of DM at $z = 7$ and 4. The view is centered on the largest galaxy in the simulation and shows a 1 h^{-1} Mpc region (comoving). The gray-scale colored particles represent the DM, while white circles in the centers of some halos show locations of the globular clusters identified in the simulation. Note that massive halos contain multiple clusters in their centers. The DM particles are colored according to the local density on a logarithmic stretch.

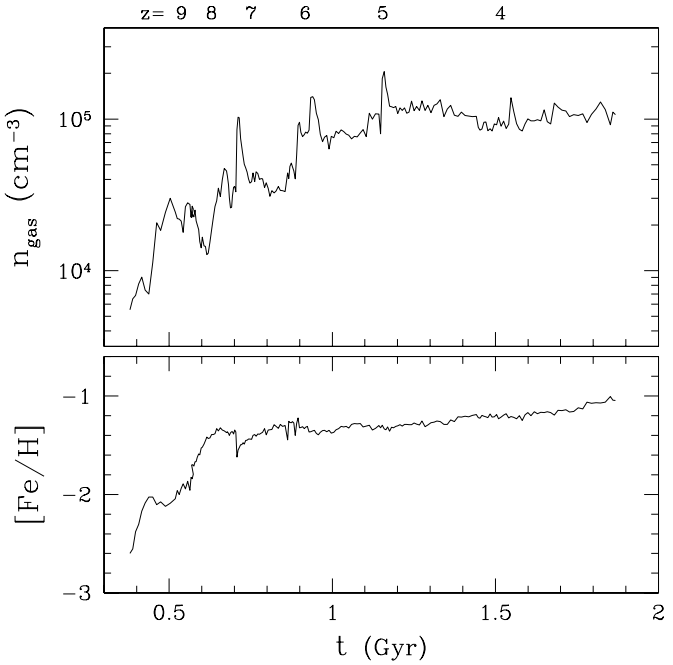

FIG. 3.—Accretion history in the central cell of the main progenitor halo. *Top*: Gas number density. The densities of DM and stars in this region are an order of magnitude smaller. *Bottom*: Iron abundance of the gas with respect to the solar value. The metallicity is due to SN II enrichment, as the contribution of SNe Ia is negligible at these epochs.

in star formation at any given time. When compared with the total gas and/or DM mass in the galaxy, the efficiency decreases by another order of magnitude. There are thus various types of GC formation efficiencies, which we consider in turn.

The detailed properties of the simulated molecular clouds depend on the threshold density, $\rho_{\rm mc}$, used to define the cloud boundary (see § 2.3). This boundary can be thought of as an external tidal limitation. The mass and size of the cloud increase with the decreasing threshold density. The cloud-scale efficiency of GC formation, which we define as $\epsilon_{\rm GC} \equiv M/M_{\rm mc}$, varies accordingly. We find that the average efficiency is about 10^{-2} for $\rho_{\rm mc} = 50\,M_\odot$ pc^{-3}, 10^{-3} to 10^{-2} for $\rho_{\rm mc} = 10\,M_\odot$ pc^{-3}, and 10^{-4} to 10^{-3} for $\rho_{\rm mc} = 1\,M_\odot$ pc^{-3}. The estimated masses of GCs, on the other hand, depend only on the properties of the cloud cores and are insensitive to the changes in the external boundary condition.

For the massive GCs with $M > 3 \times 10^5\ M_\odot$ and the associated massive molecular clouds in our fiducial model with $\rho_{\rm mc} = 1\ M_\odot$ pc^{-3}, the formation efficiency is roughly constant: $\epsilon_{\rm GC} \approx 10^{-3}$. However, if we include lower mass clusters, we find an anticorrelation with the cloud mass (Spearman correlation coefficient $r_s = -0.35$). In the range $10^5\ M_\odot < M_{\rm mc} < 10^8\ M_\odot$, the relation is $\log \epsilon_{\rm GC} = -1.6 - (0.22 \pm 0.02) \log (M_{\rm mc}/M_\odot)$. Overall, the numerical values of the efficiencies we obtain are in good agreement with observations (Harris & Pudritz 1994).

3.3. *The Global Efficiency of Globular Cluster Formation*

An important measure of the efficiency of globular cluster formation is the total mass of clusters, $M_{\rm GC}$, within a parent galactic halo. For example, in giant elliptical galaxies the ratio of the total cluster mass to the mass of stars plus the hot X-ray–emitting gas is roughly constant, $\varepsilon^b_{\rm GC} \equiv M_{\rm GC}/M_b \approx 0.0026 \pm 0.0005$ (McLaughlin 1999). This parameter can be thought of as the efficiency of the conversion of baryons into globular clusters. In massive objects the baryon mass M_b relates to the total galaxy mass M_h via the universal baryon fraction, $M_b/M_h \approx f_b \approx 0.14$. Thus, perhaps even more fundamental is the ratio of the GC mass to the total galaxy mass: $\varepsilon^t_{\rm GC} \equiv M_{\rm GC}/M_h$.

Figure 4 shows the sum of the GC masses in each halo versus the progenitor galaxy mass at the time of GC formation. There is a well-defined correlation of the form

$$M_{\rm GC} = 3.2 \times 10^6\ M_\odot \left(\frac{M_h}{10^{11}\ M_\odot}\right)^{1.13 \pm 0.08}, \qquad (6)$$

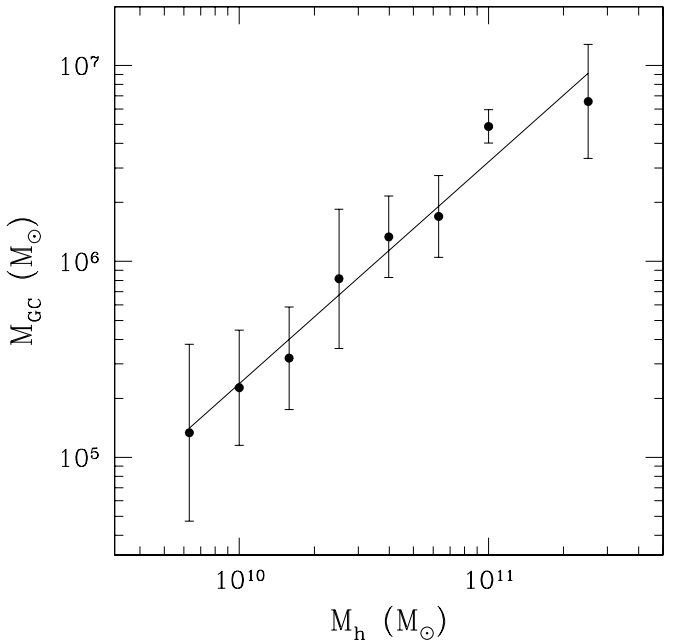

FIG. 4.—Mass of the globular cluster system within a given halo vs. the total mass of its parent halo, combined over all analyzed epochs. Filledcircles show the average in bins of width $\Delta \log M_h = 0.2$, while the error bars show the 1 σ deviations within the bin (not the error of the mean). The solid line is the least-squares fit with the slope $d \log M_{GC}/d \log M_h = 1.13 \pm 0.08$.

albeit with scatter. The global efficiency ε^t_{GC} is therefore only weakly dependent on the galaxy mass. For most halos harboring massive clusters we find $\varepsilon^t_{GC} = (2\text{–}5) \times 10^{-5}$. The global baryon efficiency is in the range $\varepsilon^b_{GC} = (2\text{–}3) \times 10^{-4}$, and it scales with the galaxy mass as

$$\frac{M_{GC}}{M_b} = 2.5 \times 10^{-4} \left(\frac{M_h}{10^{11}\ M_\odot} \right)^{0.25 \pm 0.12}. \quad (7)$$

While these values are lower than those found by McLaughlin (1999), they are in fact appropriate for a spiral galaxy like our own. McLaughlin (1999) derived $\varepsilon^b_{GC} = 0.0027$ for the Galaxy taking into account only the mass of the stellar spheroid. We are interested here in scaling with the total mass and therefore take the most recent estimate of the virial mass of the Milky Way $M_h \approx 10^{12}\ M_\odot$ (Klypin et al. 2002). The mass of the observed globular clusters is $M_{GC} = 5.2 \times 10^7\ M_\odot$ (Harris 1996), and as McLaughlin (1999) argues, this mass cannot differ from the initial mass by more than 25%. Thus, the global efficiency for the Galaxy is $\varepsilon^t_{GC} \gtrsim 5 \times 10^{-5}$, and the baryon efficiency $\varepsilon^b_{GC} \approx \varepsilon^t_{GC}/f_b \approx 4 \times 10^{-4}$. Both of these estimates agree with our derived correlations, equations (6) and (7).

The global baryon efficiency can be related to the commonly used specific frequency, $S_N \equiv N_{GC} 10^{0.4(M_V+15)}$. Taking the mean cluster mass, $2 \times 10^5\ M_\odot$, and assuming a mass-to-light ratio for old clusters, $M/L_V = 3$, we obtain $S_N = 1.2 \times 10^3 M_{GC}/M_*$. The stellar galaxy mass M_* is not a very good proxy for the baryon mass M_b at high redshifts, but it can be used for the comparison at low redshifts. Thus, our efficiency $\varepsilon^b_{GC} \approx 3 \times 10^{-4}$ corresponds to $S_N \approx 0.4$, which is indeed observed for Sc galaxies.

It is interesting also that the mass of the GC population and the maximum cluster mass in a given region strongly correlate with the local average star formation rate density: $M_{max} \propto \Sigma_{SFR}^{0.54 \pm 0.07}$ and $M_{GC} \propto \Sigma_{SFR}^{0.75 \pm 0.06}$ at $z = 3.3$, where the masses and star formation rate were estimated taking into account clusters with $M > 5 \times 10^4\ M_\odot$ and stellar particles younger than 5×10^7 yr and averaging over the cells of 7.7 physical kpc. Each averaging cell therefore represents a different progenitor galaxy in the simulation. A similar correlation was reported for the observed nearby galaxies (Larsen 2002). The interpretation of this correlation is straightforward in our model. The star formation rate depends sensitively on the mass fraction of gas in cold high-density star-forming regions (Kravtsov 2003). The massive clusters in our model are also assumed to form in such regions. Thus, both the star formation rate and the mass of the GC population are controlled by the amount of gas in the densest regions of the ISM.

3.4. *The Mass, Size, and Metallicity Distributions of the Model Clusters*

Figure 5 shows the mass function of the model clusters identified in all output epochs prior to a given redshift. At all epochs the distribution is well described by a power law $dN/dM \propto M^{-\alpha}$ at $M > 10^5\ M_\odot$. The slope α evolves slowly and saturates at $\alpha = 2.05 \pm 0.07$ for $z \leq 4$. Note that although the physical resolution of the simulation changes somewhat with time, the subgrid prescription based on the physical threshold density ensures that the cluster properties are not affected. In § 6.3 we show that the cluster mass is a fraction of the mass of the central cell of the parent molecular cloud that depends only on the physical density of the gas. The mesh in our simulation is refined in a quasi-Lagrangian fashion, so as to keep the same gas mass within a cell; thus, the cell masses and cluster masses are always similar.

In this and subsequent figures we discard the most massive cluster identified at the center of the most massive disk. Such a cluster would be identified in observations as a compact galactic nucleus rather than a distinct globular cluster.

The simplicity of the power-law shape of the mass function is deceiving, as the mass functions of clusters in individual galaxies exhibit a variety of shapes. Figure 6 shows, for example,

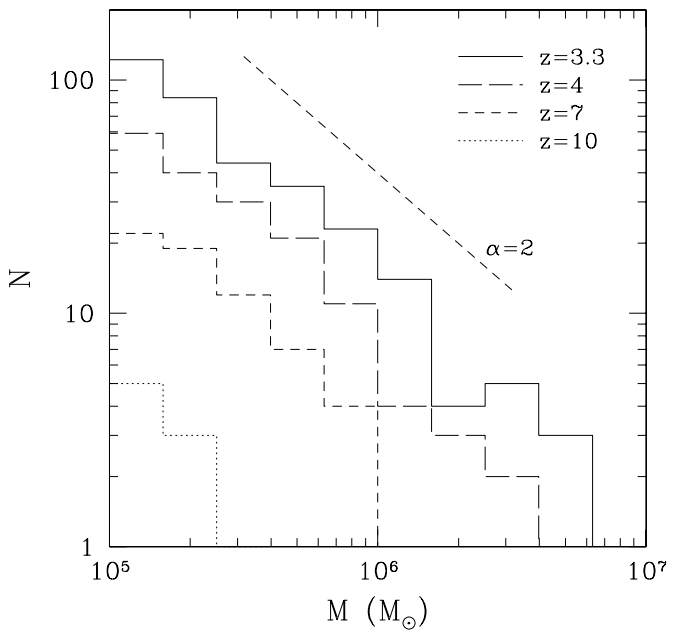

FIG. 5.—Buildup of the IMF of globular clusters. Dotted, short-dashed, long-dashed, and solid histograms show cumulative distributions at $z = 10$, 7, 4, and 3.3, respectively. The straight dashed line shows a power law, $N \propto M^{-\alpha}$, with the slope $\alpha = 2$. Note that this is the mass function of young clusters, without accounting for the effects of dynamical evolution.

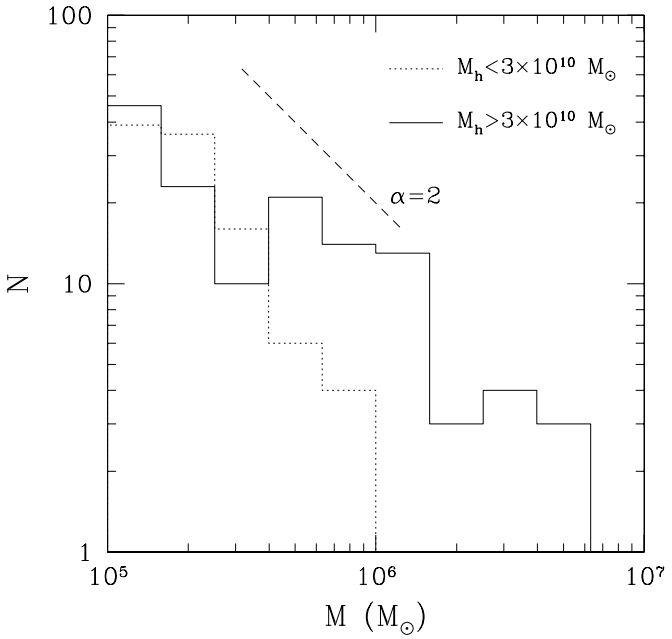

FIG. 6.—Mass function of globular clusters formed within the parent halos of mass $<3 \times 10^{10}$ (*dotted histogram*) and $>3 \times 10^{10}\ M_\odot$ (*solid histogram*) at $z = 3.3$.

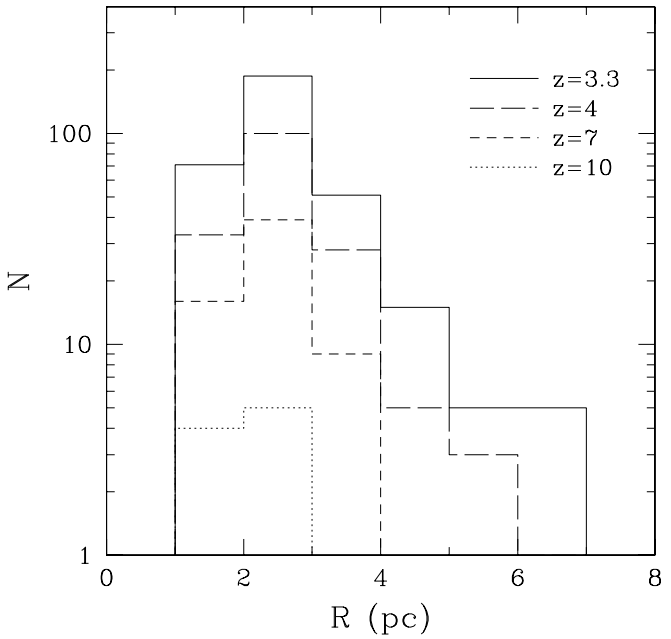

FIG. 7.—Size distributions of globular clusters at four successive epochs, using only the massive clusters, $M > 10^5\ M_\odot$.

that small halos form only clusters with $M < 10^6\ M_\odot$ with the mass function slope steeper than $\alpha = 2$, while large halos form more massive clusters with a shallower mass function. Remarkably, the convolution of the halo distribution with the distribution of clusters within each halo produces the seemingly invariant power-law mass function of globular clusters. We investigate the origin of the mass function in detail in § 4.

In contrast to this power-law function, the mass function of old Galactic and most extragalactic globular clusters has traditionally been described by a bell-shape (Gaussian) function. The mass-to-light ratio for old stars is approximately constant, and it is appropriate to use the luminosity function as a proxy to the GC mass function (GCMF). Our results can be reconciled with observations after taking into account the effects of subsequent dynamical evolution of the model clusters. Sophisticated models of the dynamical evolution, started by Spitzer and collaborators in the 1970s (see Spitzer 1987) and refined in the 1990s (e.g., Chernoff & Weinberg 1990; Gnedin & Ostriker 1997; Murali & Weinberg 1997; Vesperini & Heggie 1997; Gnedin et al. 1999), have shown that tidally truncated clusters undergo secular mass loss. The main processes shaping the GCMF are the evaporation through two-body relaxation, stellar mass loss, tidal shocking by the host galaxy, and stronger tidal truncation due to dynamical friction. Fall & Zhang (2001) have demonstrated that these processes naturally transform the initial power law into the observed truncated mass function of old GCs. Using a simple application of the above results to our model clusters, we estimate that the dynamical evolution will produce the peak and dispersion of the mass function of surviving clusters in agreement with observations. A more detailed analysis, including the orbits of clusters in merging galaxies, will be done in a subsequent study.

Figure 7 shows the distribution of the half-mass radii, calculated according to our subgrid model (eq. [4]). As with the masses, the cluster sizes do not vary systematically with the formation redshift and have consistent distributions at all epochs. In this and the following figure we plot only the massive clusters, $M > 10^5\ M_\odot$, expected to survive the dynamical evolution.

The model size distribution is generally similar to the observed sizes of the Galactic GCs (e.g., van den Bergh 1996). The differences at the smallest and largest ends can be due to the following effects. The adiabatic expansion condition may not apply to the most massive clusters, which would then be larger. The dynamical evolution effects, on the other hand, would shrink the clusters and fill the range $R < 1$ pc. Furthermore, some of the surviving clusters with $M < 10^5\ M_\odot$ may contribute to the smallest size bin as well.

By construction, our constant-density subgrid criterion leads to the correlation between cluster masses and sizes, $R \propto M^{1/3}$. Recent observations (Zepf et al. 1999; Larsen 2004) suggest that the sizes of young massive star clusters are almost independent of their masses and show weaker correlation, $R \propto M^{0.1}$. This implies either that the massive star clusters form with intrinsically higher densities or that the low-mass clusters expand more than we assumed following the loss of the remaining gas in the star-forming cores. For example, Ashman & Zepf (2001) suggested that the formation efficiency ϵ increases with the binding energy of the molecular cloud. It might therefore be useful to define two formation efficiencies: the mass conversion efficiency ϵ_M in equation (3) and the expansion efficiency ϵ_R in equation (4). As we have argued in § 2.4, ϵ_M cannot be much different from 0.5–0.6, but ϵ_R can, in principle, scale with the cluster mass. The observed trend can be explained by $\epsilon_R \propto M^{0.2}$. We do not discuss these complications further in this paper, but they should be addressed in future work.

Figure 8 shows the distribution of cluster metallicities, which is remarkably similar to the metal-poor part of the Galactic cluster distribution (see Table 1). Interestingly, we do not find any correlation between the mass and metallicity of globular clusters. The Spearman rank correlation coefficient for the cumulative distribution at $z \approx 3.3$ is $r_s = -0.06$, which is consistent with no correlation. Similarly, there is no correlation for the Galactic GCs (Djorgovski & Meylan 1994). The absence of the mass-metallicity correlation may be due to a wide range of gas metallicities in the star-forming regions. As we mentioned above, this also explains the lack of a well-defined age-metallicity correlation.

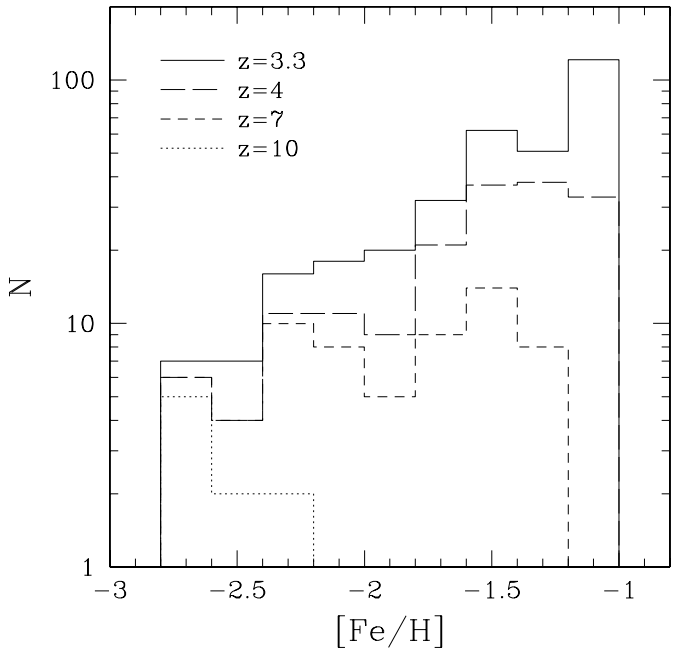

FIG. 8.—Metallicity distributions of globular clusters at four successive epochs, using only the massive clusters, $M > 10^5\ M_\odot$.

At the high redshifts considered here, most of the metals are contributed by SNe II that underproduce iron compared to the α-peak elements. In order to calculate the fraction of ejected metals contributed by iron, $\eta_{\rm Fe}$, we use the iron yields of Woosley & Weaver (1995), integrated over the Miller & Scalo (1979) IMF in the range 12–40 $M_\odot$. For the intermediate "case B" yield models and the assumed solar ratio of iron to hydrogen of 1.8×10^{-3} by mass (Anders & Grevesse 1989), we obtain $\eta_{\rm Fe}\approx 0.6$. This estimate is consistent with the enhanced ratios $[\alpha/{\rm Fe}]\approx 0.3$ observed for the GCs in the Galaxy (Carney 1996; Lee & Carney 2002; Smith et al. 2002), M87 (Cohen et al. 1998), and M49 (Cohen et al. 2003). The conversion from the total metallicity due to SNe II to the iron abundance is $[{\rm Fe/H}] = \log(\eta_{\rm Fe}Z_{\rm II}/Z_\odot)$.

Table 1 compares the medians and the 25% and 75% quartiles of the size and metallicity distributions of the model clusters against the corresponding distributions for the Galactic GC (Harris 1996). There is good agreement between our predictions and the observations. It is plausible that small discrepancies for the smallest sizes and highest metallicities can be explained by subsequent evolution of the cluster population at $z < 3$, which we discuss in § 6.1. Note that the evolution can also modify the quartiles of the distribution. We therefore show in Table 1the quartiles both for all Galactic clusters and for the clusters with metallicities in the same range as in our model (i.e., $[{\rm Fe/H}] < -1$). It is also interesting that, in agreement with observations, no clusters are formed with very low (Population III) metallicities.

Note that at all epochs the dynamical time of the parent molecular cores is very short ($\sim10^6$ yr), which means that the galactic gas is preenriched even before the first clusters form. It follows then that the oldest globular clusters do not contain the oldest stars in the Galaxy.

The lack of the metal-rich clusters in our model compared to the Galactic clusters (e.g., Table 1) is likely to be explained by the clusters forming in the higher metallicity gas at $z < 3$ (see § 6.1), not accounted for in our analysis. It should be noted, however, that a significant spread in metallicity distributions exists for different galaxies (e.g., Harris 2001) and certain differences with the simulated system are expected. This issue can be addressed in future studies by simulating GC systems in a number of galaxies.

4. THE ORIGIN AND UNIVERSALITY OF THE GLOBULAR CLUSTER MASS FUNCTION

One of the most important characteristics of GC systems is the mass function. Interestingly, the mass function derived in the simulation is similar to the mass function of molecular clouds in our and external galaxies, $dN/dM \propto M^{-\alpha}$ with $\alpha = 1.4$–2 (e.g., Solomon et al. 1987; Wilson et al. 2003). It is also similar to the high-redshift mass function of DM halos in the hierarchical CDM cosmology (Press & Schechter 1974; Sheth & Tormen 1999). In this section we investigate the origin of the GCMF in relation to the mass function of giant molecular clouds and parent halos.

Gnedin (2003) used a simple semianalytic model in which a single massive cluster dominates the mass of the GC system within a progenitor halo: $M_{\rm max} \lesssim M_{\rm GC} \approx \varepsilon_{\rm GC}^b f_b M_h$ (e.g., § 3.3). The model implies that the shape of the high-mass tail of the GCMF simply reflects the shape of the mass function of progenitor halos of the Milky Way at high redshifts. This direct connection between the cluster and halo mass functions is due to the assumption that GC properties are determined solely by the mass of their parent halo. This key assumption can be tested against the results of our simulation.

We find indeed that the most massive cluster contributes a significant fraction of the total cluster mass. The average for all halos is $M_{\rm max} \approx 0.6 M_{\rm GC}$. In § 3.3 we have shown that $M_{\rm GC}$ is roughly proportional to the parent galaxy mass, and therefore a similar relation exists for the most massive clusters:

$$M_{\rm max} = 2.9\times10^6\ M_\odot \left(\frac{M_h}{10^{11}\ M_\odot}\right)^{1.29\pm0.12}. \qquad (8)$$

However, a significant scatter around this average relation is such that for a given halo the masses of individual clusters

TABLE 1
THE QUARTILES OF THE SIZE AND METALLICITY DISTRIBUTIONS OF THE MODEL AND GALACTIC GLOBULAR CLUSTERS

Parameter	R_h(25%)	R_h(50%)	R_h(75%)	[Fe/H](25%)	[Fe/H](50%)	[Fe/H](75%)
$z = 10$	1.9	2.0	2.3	−2.7	−2.6	−2.5
$z = 7$	2.0	2.4	2.7	−2.2	−1.8	−1.6
$z = 4$	2.0	2.4	2.9	−1.8	−1.5	−1.2
$z = 3.3$	2.0	2.3	2.9	−1.7	−1.4	−1.1
MW, [Fe/H] < −1	1.2	2.8	4.8	−1.8	−1.6	−1.4
MW, all	0.7	2.4	4.0	−1.7	−1.4	−0.7

can vary by a factor of 3. Thus, the mass function of GCs does not follow directly from the mass function of their parent halos.

Instead, we find that the overall shape of GCMF in our model is determined by both the mass function of progenitor halos *and* the mass function of molecular cloud cores within individual halos. The latter, in turn, is determined by the structure of the galaxy disks and in particular by the density probability distribution function (PDF).

The shape of the PDF has been studied in several numerical simulations of the turbulent ISM. A lognormal distribution is thought to be a generic feature of *isothermal* turbulent flows (e.g., Vazquez-Semadeni 1994; Padoan et al. 1997; Vázquez-Semadeni et al. 2000). For nonisothermal supersonic flows Scalo et al. (1998) found that the PDF is a power law of density, although Nordlund & Padoan (1999) argued that even in this case the PDF can be described equally well by a power law or a lognormal function. The lognormal shape is likely to be due to the chaotic nature of the supersonic turbulent flows, characterized by numerous random convergent flows and shocks. The evolution of individual gas elements can be thought of as a random walk in density leading to the lognormal equilibrium distribution (Elmegreen 2002).

For the heating/cooling rates adopted in our simulation the gas at densities $\rho_g \gtrsim 5\ M_\odot\ \mathrm{pc}^{-3}$ cools efficiently to the lowest allowed temperature ($T_{\min} = 300$ K) and is therefore nearly isothermal. Accordingly, we expect the PDF in the simulation to be lognormal. The width of the lognormal PDF is proportional to the rms Mach number of gas clouds (Padoan et al. 1997), which increases with time in the hierarchically assembled galaxies. Thus, we expect the PDF to widen with decreasing redshift.

Figure 9 shows the density PDF measured in the simulation at $z = 7$, 4, and 3.3, using only the highest refinement level ($l = 9$) cells that cover the galactic disks and include the sites of GC formation. The lognormal distribution provides a very good fit to the high-density tail of the PDF at $\rho > 1\ M_\odot\ \mathrm{pc}^{-3}$ (see also Wada & Norman 2001; Kravtsov 2003):

$$\frac{dN}{d\log\rho} \propto \exp\left[-\frac{(\log\rho - \log\rho_0)^2}{2\sigma_\rho^2}\right]. \quad (9)$$

The characteristic density ρ_0 and the dispersion σ_ρ of the lognormal PDF vary with redshift. The characteristic density decreases from $\log\rho_0 \approx 1.8$ at $z = 8$ to $\log\rho_0 \approx 0.08$ at $z = 3.3$, while the width of the distribution σ_ρ increases from 0.46 to 0.85 at the same redshifts. The evolution in this redshift interval can be fitted by $\log\rho_0 = 3.30 - (1.41 \pm 0.02)[10/(1+z)]$ and $\sigma_\rho = 1.23 - (0.83 \pm 0.05)[(1+z)/10]$.

Figure 9 shows also that over a limited density range, $1 < \log\rho < 3$, the PDF can be described by a power law

$$\frac{dN}{d\log\rho} \propto \rho^{-n}, \quad (10)$$

with $n = 1.08 \pm 0.06$ (for $z = 4$). Over a wider range of densities, however, the lognormal function is a somewhat better description of the PDF. For instance, the power-law slope becomes steeper with increasing density: we find $n = 1.26 \pm 0.08$ for $\log\rho > 1.5$ and $n = 1.41 \pm 0.13$ for $\log\rho > 2$. The latter range includes the molecular cloud cores in which the massive clusters ($M > 10^5\ M_\odot$) form in our model.

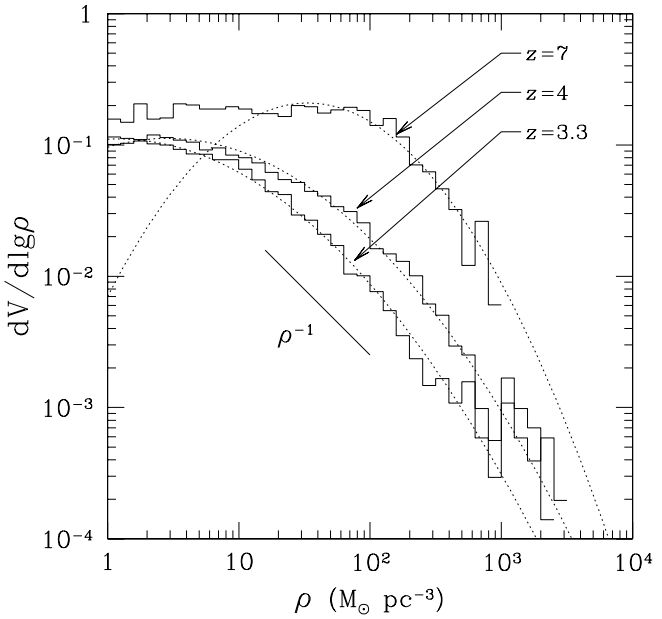

FIG. 9.—Probability distribution functions of the gas density (fraction of the total volume occupied by the cells in a given density range) for the highest level of refinement at $z = 7$, 4, and 3.3. The dotted lines show the lognormal fits to the highest density tails of the distribution, in the range 1–$10^3\ M_\odot\ \mathrm{pc}^{-3}$. The straight lines show the slopes $dV/d\log\rho \propto \rho^{-1}$ and $\rho^{-1.5}$.

We should note that the molecular clouds in the simulation are only marginally resolved. Their temperature and structure depend on the uncertain physics such as the presence of dust, cooling due to metals, UV heating by nearby stars, and radiative transfer. The form of the PDF can depend on these properties, and at this point we cannot reliably differentiate between lognormal and power-law mass functions. However, the difference between the two at the interesting densities is quite small and is not critical for our discussion.

Globular clusters in our model form only in the highest density cores of the identified molecular clouds that represent a subset of all high-density cells. Nevertheless, we find that the PDF of the cores (or density peaks) is similar to the overall cell PDF at $\log\rho > 0$. The Kolmogorov-Smirnov test of the unbinned probability distributions shows that the differences between the core PDF and the cell PDF are not statistically significant. At all epochs the probability that the two PDFs are drawn from the same distribution is at least 13%. This indicates that the density PDF of the cores is also described by the same lognormal distribution. The density of each core determines the mass of the GC it hosts. The density PDF of the cores thus determines the GCMF.

Given our subgrid model, the cluster mass scales with the core gas density as $M \propto \rho^{3/2}$ (eqs. [3] and [4]). For a power-law density PDF the expected cluster distribution is $dN/dM \propto M^{-1-2n/3}$, or $\alpha = 1 + 2n/3$. For $n = 1$ this gives the slope $\alpha = 5/3 \approx 1.7$, while for $n = 1.4 \pm 0.13$, appropriate for the highest density tails of the PDF and the massive clusters, $\alpha = 1.94 \pm 0.09$, in good agreement with the mass function slope seen in Figure 5. Therefore, we can expect a relatively shallow, $\alpha \approx 1.7$, mass function for the small-mass clusters forming in lower density cores and the steep, $\alpha \approx 2$, mass function for massive globular clusters forming in the densest regions of the disk. The range of slopes derived in our model is in close agreement with observations (Elmegreen & Efremov 1997; Zhang & Fall 1999; de Grijs et al. 2003; Anders et al. 2004).

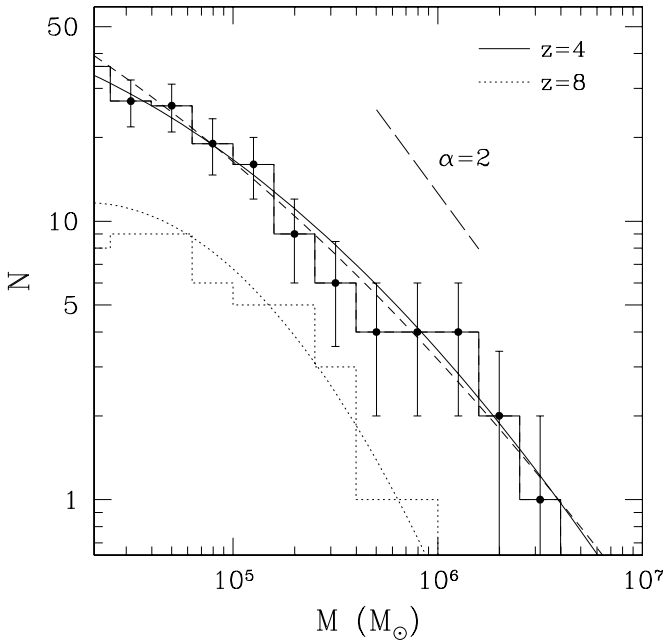

FIG. 10.—Mass function of globular clusters forming at two epochs (*histograms*) with the superimposed fit (*smooth solid and dashed lines*) from the density PDF (eq. [11]). The error bars represent Poisson errors $\propto N^{1/2}$. The dashed line shows the mass function calculated from the density PDF of the lower, $l = 8$, level of refinement normalized to the same total number of clusters.

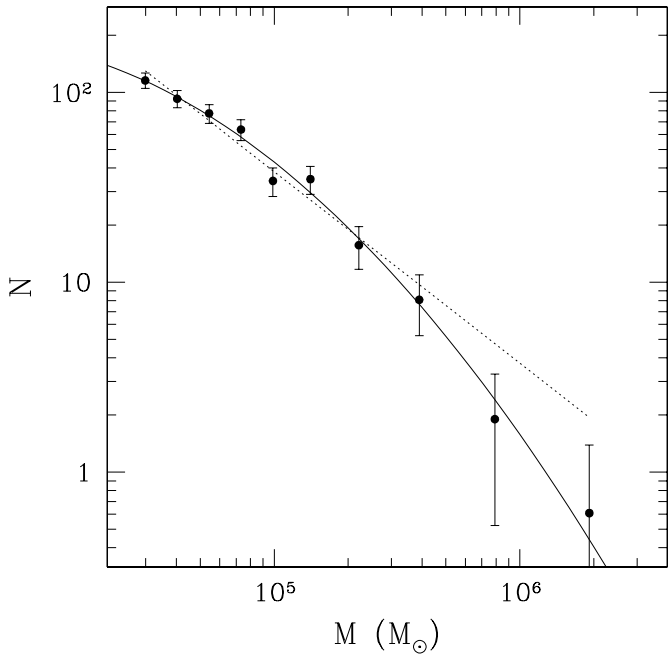

FIG. 11.—Mass function of young (age 25 Myr $< t <$ 160 Myr) star clusters (*filled circles with error bars*) in NGC 4038/4039 (the "Antennae"), as derived by Zhang & Fall (1999), and the best fits of the power-law (*dotted line*) and lognormal (*solid line*) mass distributions.

From our analysis above it is clear that the power law is not a unique description of the mass function. The lognormal shape of the density PDF implies the lognormal GCMF:

$$\frac{dN}{d\log M} = N_0 \exp\left[-\frac{(\log M/M_0)^2}{2\sigma_M^2}\right], \qquad (11)$$

with $\sigma_M = (3/2)\sigma_\rho$ and $M_0 = M(\rho_0)$ using equation (3). Figure 10 shows the mass function of clusters at $z = 8$ and 4 along with the lognormal function calculated from the best fit to the density PDF. In other words, the smooth lines in the figure represent not fits to the mass function, but the fits to the PDF converted to the mass function using our subgrid model. The lognormal mass function may thus be a reasonable choice in fitting observed luminosity and mass functions of young clusters when a simple power law does not provide a good fit.

The parameters of the distribution, M_0 and σ_M, follow directly from the parameters of the density PDF. As redshift decreases, the characteristic peak ρ_0 decreases and the dispersion σ_ρ increases. While their exact values at a given redshift may be specific to our simulated galaxy, i.e., depend on the environment, the anticorrelation between the parameters may be more general. We find the following relation, which can be tested by future simulations and observations:

$$\log M_0 = (6.2 \pm 0.5) - (2.8 \pm 0.5)\sigma_M. \qquad (12)$$

These results apply to the mass function of young stellar clusters not modified by dynamical evolution.

In order to illustrate that the lognormal distribution can fit the observations, we plot in Figure 11 the mass function of young (age 25 Myr $< t <$ 160 Myr) stellar clusters in NGC 4038/4039 (the "Antennae"), as derived by Zhang & Fall (1999). This figure shows that the lognormal function describes the observed mass function as well as the power law. The best-fit power-law slope is $\alpha = 2.01 \pm 0.07$ with the reduced $\chi^2 = 1.17$, while for the lognormal fit $\chi^2 = 0.68$. The parameters of the fit, $\log M_0 = 3.7 \pm 0.4$ and $\sigma_M = 0.73 \pm 0.12$, are in reasonable agreement with the derived relation given by equation (12), especially if we take into account the difference in redshifts, metallicity, and environment.

The results presented in this section indicate that the observed luminosity and mass functions of young clusters could be described by a power law owing to the limited range of luminosities typically probed in observations ($\sim$2–4 mag or only about a factor of 10–40 in mass; Elmegreen & Efremov 1997; Whitmore 2000). If our results are correct, the prediction would be that the power-law slope α should steepen at the highest cluster masses: $M \gtrsim 10^7\ M_\odot$. Interestingly, the lognormal mass function implies that there exists a maximum cluster mass at any given epoch. This is an important conclusion as it may explain the characteristic masses of clusters in the Local Group.

5. NUMERICAL CONVERGENCE

The resolution of the simulation in any numerical study invariably places constraints on the validity of the results. The spatial and mass resolution of the gas element in the adaptive mesh simulation is set by the maximum level of refinement. In our simulation $l_{\max} = 9$ was determined by the available computational resources. We can check, however, how the results would change if we limited the maximum level to $l = 8$. This corresponds to factor of 8 lower mass resolution and factor of 2 larger cells.

We find that the density PDF of the $l = 8$ cells can be well fitted by a lognormal function but with a correspondingly lower characteristic density ρ_0. The dispersion σ_ρ is consistent with that for the $l = 9$ level within the errors. The mass function resulting from the $l = 8$ density PDF is therefore somewhat steeper than for the $l = 9$ cells because M_0 is lower and the same mass interval of GCs falls on the steeper part of the lognormal

function. The difference, however, is only apparent at very low masses ($M \lesssim 3 \times 10^4\ M_\odot$).

The dashed line in Figure 10 shows the cluster mass function expected for the density PDF of the $l = 8$ cells normalized to the same number of clusters as the $l = 9$ mass function. It fits the histogram of the model clusters equally well. The deviation only becomes significant at $M < 3 \times 10^4\ M_\odot$. Thus, the shape of the derived mass function converged at masses higher than $3 \times 10^4\ M_\odot$.

Our assumption that each molecular cloud forms only one cluster may also affect the low-mass end of the mass function. If in reality the cloud fragments into several self-gravitating cores, then smaller clusters may form on the periphery of the cloud in addition to the larger central cluster. However, as we show in the next section, these additional small clusters are likely to be quickly dissolved, so that in the end the mass function of the surviving massive clusters remains the same.

6. DISCUSSION

6.1. *Evolution of Globular Clusters at Lower Redshifts*

In the preceding sections we analyze the formation of globular clusters at $z \gtrsim 3$. Although the limited computational resources did not allow us to continue the simulation at the same resolution to lower redshifts, in this section we conjecture on the possible evolution of cluster population at later epochs.

Analysis of our simulations hints that massive molecular clouds needed for cluster formation are built in gaseous spiral arms. Their formation may be enhanced in mergers between gas-rich gas disks. For example, as we note in the caption of Figure 1, the gas disk shown in this figure is actually in a state of very active accretion and merging. For instance, the two cold dense clumps clearly seen in the temperature map are two satellite galaxies in the process of merging with the disk. The mass of the parent halo of the disk in Figure 1 increases by a factor of 20 between redshifts of 10 and 4 (a period of only $\sim$1 Gyr; see § 2.2).

It is commonly thought that galaxy mergers create conditions conducive to bursts of star formation and star cluster formation, as evidenced by the starbursting galaxies (Kennicutt 1998; Larsen 2002). In particular, mergers stir and compress the interstellar gas creating the high-pressure environments in which dense clouds and massive stellar clusters can form (Elmegreen 2002). Without the mergers, star formation proceeds in a quiescent mode (e.g., Abadi et al. 2003).

The high rate of accretion and merging cannot be maintained at lower redshifts. Statistically, the CDM halo merger rate at $z \lesssim 4$ decreases rapidly as $(1 + z)^{-2.5}$ (Gottlöber et al. 2001). In addition, as galaxies evolve, most of the gas will be converted to stars so that the large reservoir of gas needed to build up giant molecular clouds may not be available. Therefore, if galaxy mergers are connected to GC formation, a high merger rate between gas-rich galaxies at $z > 3$ would lead to an almost continuous cluster formation. At lower redshifts, on the other hand, mergers become rare and the merging galaxies are gas deficient compared to their high-redshift progenitors. Most of the subsequent formation of stellar clusters may thus be limited to a single last major merger event. This, for example, could explain the bimodality of cluster colors observed in many elliptical galaxies.

Finally, somewhat paradoxically, the globular clusters formed at high redshifts may have a significantly higher chance of survival until the present than clusters formed at later epochs. The clusters in our model form in extremely high density environments within the galactic disks. Strong tidal forces in such regions are likely to disrupt clusters quickly, unless they are located at the very center of the parent galaxy or are ejected from the disk by a dynamical process shortly after formation. As only a fraction of clusters form in the centers of progenitor galaxies, the latter mechanism should operate in order for the old metal-poor clusters to survive until the present.

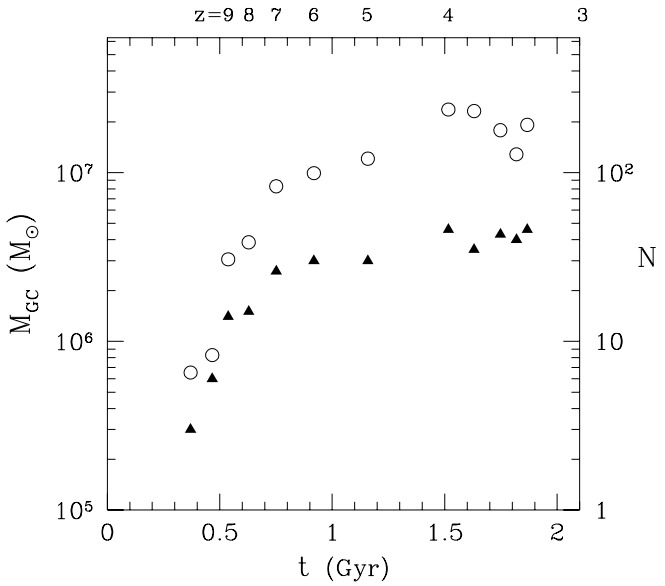

FIG. 12.—Number of clusters (*triangles*) and total mass in clusters (*circles*) formed at each simulation output according to our model. The number of sites of cluster formation reaches a plateau at $z \approx 4$ and may decline at lower redshifts.

Frequent violent mergers at high redshifts may be just such a mechanism. Mergers disrupt the disks of the progenitor galaxies with their existing stellar populations and impart a large amount of orbital energy in the surviving clusters. The high-energy orbits would allow globular clusters to spend most of the time in the relatively low density regions of the halo, outside the main disk. Mergers could be responsible for a spheroidal distribution of the GC systems, even though the clusters actually form within the disks of the progenitor systems. At low redshifts, on the other hand, star clusters, even if they continue to form, may not be able to escape the disk quickly enough to avoid disruption.

The effects discussed above may result in the preferred, albeit extended, epoch of GC formation at $z_{GC} \sim 2$–12 ($t_{GC} \sim 0.3$–3 Gyr for the adopted cosmological model). We cannot prove this conjecture directly in our present simulations, although one may argue that there are indications of this trend at $z \sim 3$–4. Figure 12 shows that the total mass of the GC population and the number of clusters forming at a given epoch increase until $z \approx 4$ and then saturate at a constant value at lower redshifts.

Note that Figure 12 should be interpreted with caution. Since clusters are not formed self-consistently during the simulation run time but rather calculated a posteriori, it is impossible to compute the rate of their formation. In a self-consistent treatment, clusters forming at a given epoch may exhaust the supply of gas in the regions conducive to cluster formation and prevent the formation of new clusters in the same place. In our current analysis, on the other hand, clusters at subsequent epochs can, in principle, form from the same gas. At the high redshifts that we considered, the gas distribution changes sufficiently quickly and the rate of accretion of new gas is very high, so that the epochs separated by tens of millions of years can be safely considered independent. This may not be true for nearby epochs. The flattening of M_{GC} and N_{GC} in this figure can be interpreted as the fact

that no new sites for cluster formation are created. Unfortunately, this is the best estimate of the formation rate that we can provide with our current simulation. Our future work will address the formation of star clusters at low redshifts directly.

To summarize, we conjecture that the formation of GCs at $z \lesssim 2$–3 can be associated with the increasingly rare merger events and would thus be progressively episodic. The merger rates derived from cosmological simulations (Gottlöber et al. 2001) indicate that on average galactic halos experience one to four major mergers with the mass ratio >0.2 at $z < 2$. Two broad evolutionary scenarios can be envisioned in this picture. If the last major merger occurs early ($z_{\rm merge} \gtrsim 2$), not too far from the preferred epoch of GC formation, we would expect a continuous change of the cluster properties. If, on the other hand, the galaxy experiences the last major merger late ($z_{\rm merge} \lesssim 1$), with a substantial gap between $z_{\rm merge}$ and $z_{\rm GC}$, the distribution of properties of the resulting cluster populations may be bimodal. The bimodality in this case would reflect a considerable change in the galactic environment (e.g., the metallicity of gas) during the interval $\Delta z = z_{\rm GC} - z_{\rm merge}$. The latter scenario is particularly relevant to the formation of large elliptical galaxies.

6.2. *Comparison with Previous Work*

Several recent studies explored the formation of globular clusters in the context of hierarchical cosmology using both numerical simulations and phenomenological semianalytic models. Here we discuss and compare the specifics and results of our study to the previous similar efforts.

Weil & Pudritz (2001) used a Tree-SPH simulation of the τCDM ($\Omega_0 = 1$) cosmology to study the large-scale distribution of giant gas clouds at $z \lesssim 1$ in a $32\,h^{-1}$ Mpc box. The authors analyzed collisions of baryonic clumps (clouds) in small-mass DM halos within the context of the agglomeration model of Harris & Pudritz (1994). They found a characteristic power-law spectrum of cloud masses, $dN/dM_{\rm mc} \propto M_{\rm mc}^{-1.7}$, similar to the mass function of molecular clouds and young star clusters. The mass function of clouds and globular clusters in our model is consistent with their result. The detailed comparison, however, is not possible as the simulations of Weil & Pudritz (2001) did not include star formation and the cooling of gas below 10^4 K. In addition, their low spatial resolution ($\sim$1 kpc) prevented any detailed study of the inner structure of the clouds, as well as the density distribution and mass spectrum of clusters within individual galaxies.

Recently, Bromm & Clarke (2002) used a Tree-SPH simulation to study the collapse and fragmentation of gas during the evolution of a single dwarf galaxy $\sim 10^8\,M_\odot$ at $z \lesssim 24$. The simulation assumed that the gas was preenriched to the metallicity of $10^{-2}\,Z_\odot$, which allowed the gas to cool to $\sim$1000 K, and used sink particles to follow the collapse of the gas in the highest density ($n > 10^3$ cm^{-3}) regions. The authors identified six gas clumps with masses in the range from 4×10^4 to $2 \times 10^7\,M_\odot$, each associated with a separate small-mass DM halo. They concluded that the characteristic mass of GCs is determined by the characteristic mass of DM halos forming at $z \gtrsim 10$.

The implicit assumption behind their conclusion is that the conditions for cluster formation exist only at the earliest stages of galaxy formation, prior to reionization. The results of our study show that, although the first GCs may form at $z > 10$, the conditions for cluster formation become more favorable at lower redshifts when more gas accumulates in the disks of the progenitor halos. Reionization does not affect significantly the formation of clusters in the relatively massive halos ($M_h \gtrsim 10^{10}\,M_\odot$). Again, it is difficult to make a more detailed comparison, given the very different setup of numerical simulations and physical processes included. Yet, it is worth noting that the gas density in the most massive clump in the simulation of Bromm & Clarke (2002; see their Fig. 3) is well below the density of DM. The average gas density at the resolution limit in the inner 10 pc is only $\sim 10\,M_\odot$ pc^{-3}, lower than the observed density of globular clusters (§ 2.4). The expected mass loss after cluster formation would reduce the cluster density even further. It is likely that such clumps are still insufficiently dense to form real globular clusters.

In contrast, the gas density at the sites of GC formation in our simulation is considerably higher ($\gtrsim 100\,M_\odot$ pc^{-3}) and is typically at least an order of magnitude larger than the local density of DM. We further assume that the clusters form only at densities $\rho > 10^4\,M_\odot$ pc^{-3} within the collapsing isothermal molecular cores. The fact that GC formation sites are strongly baryon-dominated explains the absence of DM halos around globular clusters. Bromm & Clarke (2002), on the other hand, conjecture that DM hosts of globular clusters dissolve via violent relaxation before the cluster forms, while the baryonic cores survive.

Both of the above studies attribute the shape of the GC mass function to the distribution of their parent DM halos. Our results indicate that the situation is more complex. We have shown that the shape of the GCMF is determined by *both* the mass function of the parent halos and the mass distribution of clusters within a single halo (§ 4).

Beasley et al. (2002) extended the semianalytical model of galaxy formation GALFORM to include a phenomenological prescription for GC formation. The model assumed that a constant fraction of stellar mass, ε, would be in the form of GCs. The blue (metal-poor) clusters were associated with the quiescent mode of star formation, while the red (metal-rich) clusters were assumed to form during starbursts. The parameters, $\varepsilon = 0.002$ for blue clusters and $\varepsilon = 0.007$ for red clusters, were set to agree with the observed color distribution of the elliptical galaxy NGC 4472. However, Beasley et al. (2002) truncated the formation of blue clusters arbitrarily at $z = 5$ to create a distinctly bimodal distribution of colors in their model. In addition, they find an age-metallicity correlation for their model clusters, which is a definite prediction of semianalytical models. In contrast, our simulation follows the gas dynamics and metal enrichment self-consistently and does not predict any clear age-metallicity relation.

6.3. *Alternative Subgrid Models*

The results we presented are based on a particular subgrid model. The main features of the adopted model are the assumption of the isothermal cloud structure within the density peak of each molecular cloud and the assumption that clusters form with a fixed efficiency at densities above a constant density threshold (see § 2.4).

Here we consider alternative subgrid models and show that they either can be reduced to the model we use or cannot successfully reproduce the mass function of GCs. Specifically, we consider the following alternative functions for the cluster formation threshold: (1) the Jeans mass, (2) the thermal pressure, and (3) the total pressure contributed by thermal and turbulent motions. The size of the star-forming core, and therefore the cluster mass, is determined differently by a threshold value of each of these functions.

In general, an alternative subgrid model can have a threshold parameter that varies with the radius differently from the

isothermal gas density profile, $\rho_g \propto r^{-2}$. It is likely, however, that in an isothermal cloud any function of interest would be a power law, $f(r) \propto r^{-a}$. The star formation radius corresponding to the threshold value $f_{\rm CSF}$ is then determined by $f(R_{\rm CSF}) = f_{\rm CSF}$.

Since in the simulation we can only measure the parameter $f_{\rm cell}$ averaged over the cell volume, we need to consider the volume average

$$f_{\rm av}(<r) = \frac{1}{V(r)} \int_0^r f(r) 4\pi r^2 \, dr = \frac{3}{3-a} f(r). \quad (13)$$

The measured parameter is $f_{\rm cell} \equiv f_{\rm av}(<R_{\rm cell})$. Therefore, the subgrid distribution is

$$f(r) = \frac{3-a}{3} f_{\rm cell} \left(\frac{r}{R_{\rm cell}} \right)^{-a}. \quad (14)$$

The radius of the star-forming core is

$$R_{\rm CSF} = R_{\rm cell} \left(\frac{3-a}{3} \frac{f_{\rm cell}}{f_{\rm CSF}} \right)^{1/a}, \quad (15)$$

and the enclosed mass is

$$M(R_{\rm CSF}) = M_{\rm cell} \left(\frac{3-a}{3} \frac{f_{\rm cell}}{f_{\rm CSF}} \right)^{1/a}, \quad (16)$$

where $M_{\rm cell} \equiv (4\pi/3)\rho_{\rm cell} R_{\rm cell}^3$ is the amount of gas within a sphere embedded into the cell. Including the efficiency of star formation ϵ, the stellar mass is $M_* = \epsilon M(R_{\rm SF})$ and stellar radius is $R_* = R_{\rm SF}/\epsilon$.

The Jeans mass is a critical mass of a cloud of density ρ_g and temperature T that is unstable to gravitational instability, $M_{\rm J} \propto T^{3/2} \rho_g^{-1/2}$. For isothermal molecular clouds with $T \approx$ const and $\rho_g \propto r^{-2}$, a threshold in $M_{\rm J}$ reduces to a corresponding threshold in ρ_g, i.e., our original model. Similarly, the thermal pressure criterion $P_{\rm th} \propto \rho_g T$ reduces to the density criterion.

The only variable independent of the gas density, at least in principle, is the turbulent velocity dispersion, σ. Turbulence in the galactic disks is created by gravitational motions on scales larger than a single cell and reflects large-scale flows around the cloud. In the simulation, the turbulent pressure, $P_{\rm turb} = \rho_g \sigma^2$, typically dominates over the thermal by 1 or 2 orders of magnitude, so that the total pressure $P \approx P_{\rm turb}$. The velocity dispersions and sizes of the Galactic giant molecular clouds satisfy the following relation: $\sigma \propto r^{1/2}$ (Larson 1981; Brunt & Heyer 2002). If the turbulent velocity dispersion scales with the radius inside the cell as $\sigma \propto r^{1/2}$, while $\rho_g \propto r^{-2}$, then $P \propto r^{-1}$.

A reasonable fiducial value for the threshold pressure, $P_{\rm CSF}$, can be obtained from observations of the Galactic GCs. The median value of the pressure at the half-mass radius is $P_{\rm obs} \sim 10^9$ K cm^{-3}. The observable pressure in our model can be derived taking into account the postformation expansion of the cluster. Analogously to the observable density (eq. [5]), we find $P = (3/2)\epsilon^4 P_{\rm CSF}$. Setting $P = P_{\rm obs}$, we obtain the star formation threshold $P_{\rm CSF} = 5 \times 10^9$ K cm^{-3} $= 10^6 M_\odot$ pc^{-3} km^2 s^{-2}.

The velocity dispersion in a cloud is calculated directly from the gas velocities in the simulation. First, the cloud is centered on the cell of highest density. Then, the center-of-mass motion, the net radial motion, and the solid-body rotation velocity are subtracted from the velocities of the cloud cells. The remaining velocity field is free of global organized motion. The resulting velocity dispersion is close to isotropic, as expected for a clean turbulent field. We use these turbulent dispersions, σ, to calculate the turbulent pressure in the central cloud cell. Then we apply equations (15) and (16) to calculate the predicted cluster sizes and masses, using $f_{\rm cell} = \rho_{\rm cell}\sigma_{\rm cell}^2$, $f_{\rm CSF} = P_{\rm CSF}$, and $a = 1$.

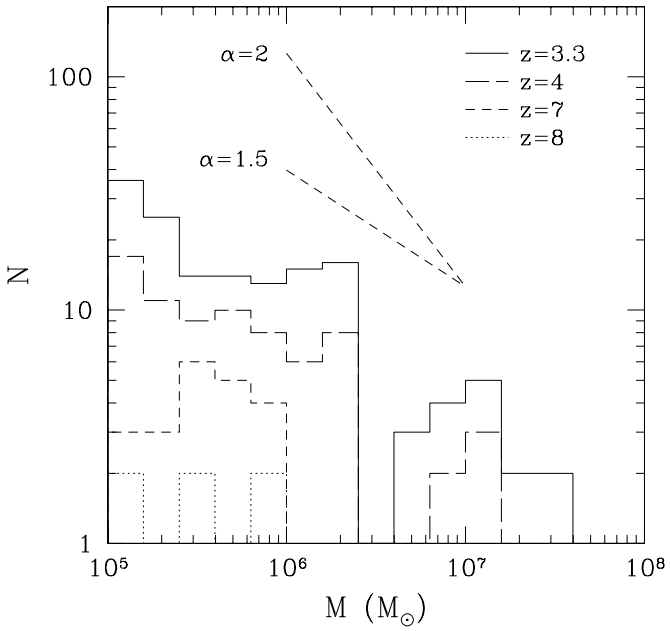

FIG. 13.—Buildup of the IMF of GCs based on the turbulent pressure criterion. Dotted, short-dashed, long-dashed, and solid histograms show cumulative distributions at $z = 8$, 7, 4, and 3.3, respectively. The straight dashed lines show two power laws, $N \propto M^{-\alpha}$. Note that the mass function is significantly shallower than that with the density criterion, $\alpha = 2$.

Figure 13 shows the cluster mass function calculated for this subgrid model, which should be compared to Figure 5. It is clear that the turbulent pressure criterion predicts a much shallower mass function than that in the density threshold model. The power-law slope is $\alpha \lesssim 1.5$. Such shallow slope is inconsistent with observations.

The value of the slope can be easily understood. According to equation (16), the cluster mass is a certain fraction of the cell mass. This fraction depends on $(P_{\rm cell}/P_{\rm CSF})^{1/a}$, and in this case $a = 1$. If the fraction can be expressed as some power of the cell mass, $M_{\rm cell}$, then the cluster mass function can be derived from the mass function of central cloud cells (uniquely determined in the simulation), and the transformation would depend on the particular subgrid model. Most of the densest cells are at the last refinement level and all have the same volume at any given epoch, so that $M_{\rm cell} \propto \rho_{\rm cell}$. In agreement with the density PDF (eq. [10]), the distribution of the central cells is roughly described by a power law

$$\frac{dN}{dM_{\rm cell}} \propto M_{\rm cell}^{-5/2} \quad (17)$$

for $M_{\rm cell} > 10^7 M_\odot$, which are the cells harboring most of the massive clusters.

Let us now derive the transformation from the cell mass to the cluster mass. The turbulent velocity does not in general scale with the cell mass, since it is caused by large-scale flows, but we still find a fairly robust correlation in the expected sense, $\sigma^2 \propto M_{\rm cell}$, to within 0.3 dex in $\log \sigma^2$. Therefore, $M_* \propto \rho_{\rm cell} P_{\rm cell} \propto M_{\rm cell}^3$. Substituting this relation into equation (17), we find

$$\frac{dN}{dM_*} \propto M_*^{-3/2}. \quad (18)$$

This is comparable to the slope seen in Figure 13 and is significantly shallower than the observed slope.

The general formalism of calculating the cluster mass function developed here gives us a powerful tool to evaluate the alternative subgrid models. Unless the transformation from the cell mass to cluster mass is the same as for the density criterion ($M_* \propto M_{\rm cell}^{3/2}$, leading to $\alpha \approx 2$), the predicted cluster mass function would deviate from the observed. The criterion based on the turbulent pressure, at least in principle independent of the density criterion, fails to reproduce the observed mass function of young star clusters.

Of course, our prescription based on a simple threshold value of a spherically symmetric function does not capture all the details of the molecular cloud physics, such as the filamentary internal structure, dust, and magnetic fields. These complications are beyond current models of galaxy formation. However, within the scope of our spherically symmetric approach to the molecular clouds, the cluster formation criterion based on the density threshold seems to reproduce the observations best.

7. SUMMARY

We have presented a study of globular cluster formation at $z > 3$ using a very high resolution cosmological simulation. The clusters in our model form in the high-density isothermal cores of giant molecular clouds in dense gaseous disks of high-redshift galaxies. The properties of globular clusters are estimated using a simple physically motivated subgrid model. Many of the observed properties of globular clusters are reproduced naturally, without fine-tuning. Our main conclusions can be summarized as follows:

1. Our results indicate that the first globular clusters in the Galaxy should have formed around $z \approx 12$ and cluster formation continued at least until $z \approx 3$.

2. Most globular clusters in our model form in halos of mass $\gtrsim 10^9\,M_\odot$. The spatial distribution of these halos at $z > 3$ is highly clustered (biased) with respect to the overall distribution of matter (§ 3.1). The high spatial bias of their parent halos explains the present more concentrated radial distribution of globular clusters relative to DM.

3. Within the progenitor systems, globular clusters form in the highest density regions of the disk: the cores of molecular clouds. In the most massive disk in the simulation, the newly formed clusters trace the spiral arms and the nucleus similarly to the young stellar clusters observed in merging and starbursting galaxies.

4. The mass function of globular clusters at birth can be approximated by a power law $dN/dM \propto M^{-\alpha}$ with $\alpha \approx 2$, in good agreement with observations of young star clusters in the Antennae. It can also be well approximated by the lognormal function. The shape of the mass function is determined by both the mass function of parent galaxies and the mass distribution of molecular cloud cores within each halo. Although the physical processes governing the evolution of the halos and molecular clouds are completely different, their mass distributions can both be approximated by the power-law functions with $\alpha \approx 1.5$–2.

5. The halo mass function arises during the hierarchical buildup of structures in the expanding universe from the initial random perturbations. The mass function of the molecular cloud cores, on the other hand, samples the underlying density PDF of the gas in the galactic disks.

6. The local efficiency of GC formation within the parent molecular cloud is $M/M_{\rm mc} \approx 10^{-3}$, with considerable scatter. The global efficiency, the ratio of the total GC mass to the baryonic mass of the parent galaxy, is $M_{\rm GC}/M_b \approx (2$–$3) \times 10^{-4}$. The mass in globular clusters scales with the total galaxy mass as $M_{\rm GC} \propto M_h^{1.1}$ (eq. [6]). These values for the formation efficiencies are in general agreement with observations (Harris & Pudritz 1994; McLaughlin 1999).

7. We find that the mass of the GC population and the maximum cluster mass in a given region strongly correlate with the local average star formation rate density: $M_{\rm max} \propto \Sigma_{\rm SFR}^{0.54\pm0.07}$ and $M_{\rm GC} \propto \Sigma_{\rm SFR}^{0.75\pm0.06}$ at $z = 3.3$. A similar correlation exists for the observed nearby galaxies (Larsen 2002). The correlation arises because both the star formation rate and mass of the GC population are controlled by the amount of gas in the densest regions of the ISM. However, it is not clear whether this correlation is general or applies only to gas-rich starbursting environments.

8. Our model predicts the lack of clear age-metallicity and mass-metallicity correlations, at least for the clusters with $[{\rm Fe/H}] \lesssim -1$. Although there is an overall trend of increasing the average metallicity with time, a significant spread of metallicities exists among different progenitor galaxies and within the ISM of each galaxy. The field stars and stellar clusters forming at a given epoch in the simulation exhibit scatter in metallicity of up to 2 orders of magnitude.

9. The distributions of sizes and metallicities of the massive ($M > 10^5\ M_\odot$) globular clusters match those of the Galactic GCs, with the exception of the largest size and the highest metallicity tail. It is plausible that these discrepancies can be rectified by dynamical evolution and the continuing formation of globular clusters at $z < 3$.

The simulation results presented in this paper directly address only formation of clusters at $z > 3$. We conjecture (§ 6.1) that the overall efficiency of GC formation and chances for their survival are significantly reduced at lower redshifts with most clusters at $z \lesssim 2$ forming in rare gas-rich galactic mergers. Although we cannot prove this with our current simulations, we argue that the preferred formation epoch of globular clusters surviving until the present is $z \sim 3$–5 (or $t \sim 1$–2 Gyr in the adopted cosmology) when the gas supply is abundant in the disks of the progenitor halos and the merger rate of the progenitors is high. All old GCs thus would appear to have similar ages.

Although the high-redshift globular clusters form in dense *gaseous* disks, most of the high-z disks are expected to merge with the Milky Way and disrupt by $z = 0$. The disrupted systems form a diffuse DM halo and contribute to the stellar halo of the host. Their clusters would share the fate of the stripped stars of the disrupted galaxies that build up galactic stellar halos and should therefore have a present-day spatial distribution similar to that of the stellar halo.

In future work, we plan to study the details of the dynamical evolution of the GC population by extending our current simulation to $z = 0$. We will incorporate our subgrid model of star cluster formation directly in the high-resolution simulations of galaxy formation.

Our present results are encouraging and demonstrate that globular clusters with properties similar to the observed clusters form naturally within young $z \gtrsim 3$ galaxy disks in the standard ΛCDM cosmology. The conditions for cluster formation appear to be widespread at $z \sim 5$, coinciding with the peak of global star formation rate. As the formation of first stars marks the end of cosmic dark ages (Rees 1997), the formation of globular clusters marks a veritable stellar renaissance of the universe.

We would like to thank L. Blitz, S. Boldyrev, M. Fall, D. Lamb, G. Meylan, E. Ostriker, J. Truran, S. van den Bergh, and S. Zepf for stimulating discussions on globular cluster formation and Q. Zhang for providing the mass function for the Antennae. We are also grateful to Nicole Papa for careful reading of the manuscript. The simulations and analyses presented here were performed on the IBM RS/6000 SP system at the National Energy Research Scientific Computing Center (NERSC) and on the Origin2000 at the National Center for Supercomputing Applications (NCSA). This work was supported by the National Science Foundation under grants AST 02-06216 and AST 02-39759 (CAREER) to the University of Chicago. O. Y. G. is supported by the STScI Fellowship.

REFERENCES

Abadi, M. G., Navarro, J. F., Steinmetz, M., & Eke, V. R. 2003, ApJ, 597, 21
Anders, E., & Grevesse, N. 1989, Geochim. Cosmochim. Acta, 53, 197
Anders, P., de Grijs, R., Fritze-v. Alvensleben, U., & Bissantz, N. 2004, MNRAS, 347, 17
Ashman, K. M., & Zepf, S. E. 1992, ApJ, 384, 50
———. 2001, AJ, 122, 1888
Bate, M. R., Bonnell, I. A., & Bromm, V. 2003, MNRAS, 339, 577
Beasley, M. A., Baugh, C. M., Forbes, D. A., Sharples, R. M., & Frenk, C. S. 2002, MNRAS, 333, 383
Boily, C. M., & Kroupa, P. 2003, MNRAS, 338, 673
Bromm, V., & Clarke, C. J. 2002, ApJ, 566, L1
Brunt, C. M., & Heyer, M. H. 2002, ApJ, 566, 289
Bullock, J. S., Kravtsov, A. V., & Weinberg, D. H. 2001, ApJ, 548, 33
Burkert, A., Truran, J. W., & Hensler, G. 1992, ApJ, 391, 651
Carney, B. W. 1996, PASP, 108, 900
———. 2001, in Star Clusters, ed. L. Labhardt & B. Binggeli (Berlin: Springer), 1
Cen, R. 2001, ApJ, 560, 592
Chernoff, D. F., & Weinberg, M. D. 1990, ApJ, 351, 121
Cohen, J. G., Blakeslee, J. P., & Côté, P. 2003, ApJ, 592, 866
Cohen, J. G., Blakeslee, J. P., & Ryzhov, A. 1998, ApJ, 496, 808
Colella, P., & Glaz, H. M. 1985, J. Comput. Phys., 59, 264
Côté, P., Marzke, R. O., West, M. J., & Minniti, D. 2000, ApJ, 533, 869
Côté, P., West, M. J., & Marzke, R. O. 2002, ApJ, 567, 853
de Grijs, R., Anders, P., Bastian, N., Lynds, R., Lamers, H. J. G. L. M., & O'Neil, E. J. 2003, MNRAS, 343, 1285
Dekel, A., & Woo, J. 2003, MNRAS, 344, 1131
Djorgovski, S., & Meylan, G. 1994, AJ, 108, 1292
Elmegreen, B. G. 2002, ApJ, 577, 206
Elmegreen, B. G., & Efremov, Y. N. 1997, ApJ, 480, 235
Fall, S. M., & Rees, M. J. 1985, ApJ, 298, 18
Fall, S. M., & Zhang, Q. 2001, ApJ, 561, 751
Ferland, G. J., Korista, K. T., Verner, D. A., Ferguson, J. W., Kingdon, J. B., & Verner, E. M. 1998, PASP, 110, 761
Freeman, K., & Bland-Hawthorn, J. 2002, ARA&A, 40, 487
Geyer, M. P., & Burkert, A. 2001, MNRAS, 323, 988
Gnedin, O. Y. 2003, in Extragalactic Globular Cluster Systems, ed. M. Kissler-Patig (Berlin: Springer), 224
Gnedin, O. Y., Lahav, O., & Rees, M. J. 2001, preprint (astro-ph/0108034)
Gnedin, O. Y., Lee, H. M., & Ostriker, J. P. 1999, ApJ, 522, 935
Gnedin, O. Y., & Ostriker, J. P. 1997, ApJ, 474, 223
Gottlöber, S., Klypin, A., & Kravtsov, A. V. 2001, ApJ, 546, 223
Gunn, J. E. 1980, in Globular Clusters, ed. D. Hanes & B. Madore (Cambridge: Cambridge Univ. Press), 301
Harris, W. E. 1996, AJ, 112, 1487
———. 2001, in Star Clusters, ed. L. Labhardt & B. Binggeli (Berlin: Springer), 223
Harris, W. E., & Pudritz, R. E. 1994, ApJ, 429, 177
Holtzman, J. A., et al. 1996, AJ, 112, 416
Hu, W., & Sugiyama, N. 1996, ApJ, 471, 542
Jungwiert, B., Combes, F., & Palouš, J. 2001, A&A, 376, 85
Kennicutt, R. C., Jr. 1998, ARA&A, 36, 189
Khokhlov, A. M. 1998, J. Comput. Phys., 143, 519
Klypin, A., Kravtsov, A. V., Bullock, J. S., & Primack, J. R. 2001, ApJ, 554, 903
Klypin, A., Zhao, H., & Somerville, R. S. 2002, ApJ, 573, 597
Kormendy, J. 1985, ApJ, 295, 73
Kravtsov, A. V. 1999, Ph.D. thesis, New Mexico State Univ.
———. 2003, ApJ, 590, L1
Kravtsov, A. V., Gnedin, O. Y., & Klypin, A. A. 2004, ApJ, 609, 482
Kravtsov, A. V., Klypin, A. A., & Khokhlov, A. M. 1997, ApJS, 111, 73
Kroupa, P., Aarseth, S., & Hurley, J. 2001, MNRAS, 321, 699
Kroupa, P., & Boily, C. M. 2002, MNRAS, 336, 1188
Larsen, S. S. 2002, AJ, 124, 1393
———. 2004, preprint (astro-ph/0403244)
Larson, R. B. 1981, MNRAS, 194, 809
———. 1996, in ASP Conf. Ser. 92, Formation of the Galactic Halo . . . Inside and Out, ed. H. Morrison & A. Sarajedini (San Francisco: ASP), 241
Lee, J., & Carney, B. W. 2002, AJ, 124, 1511
Lynden-Bell, D., & Lynden-Bell, R. M. 1995, MNRAS, 275, 429
McLaughlin, D. E. 1999, AJ, 117, 2398
McLaughlin, D. E., & Pudritz, R. E. 1996, ApJ, 457, 578
Miller, G. E., & Scalo, J. M. 1979, ApJS, 41, 513
Moore, B. 1996, ApJ, 461, L13
Murali, C., & Weinberg, M. D. 1997, MNRAS, 288, 749
Murray, S. D., & Lin, D. N. C. 1992, ApJ, 400, 265
Nakasato, N., Mori, M., & Nomoto, K. 2000, ApJ, 535, 776
Nordlund, Å. K., & Padoan, P. 1999, in Interstellar Turbulence, ed. J. Franco & A. Carraminana (Cambridge: Cambridge Univ. Press), 218
Odenkirchen, M., et al. 2003, AJ, 126, 2385
Ostriker, E. C., Stone, J. M., & Gammie, C. F. 2001, ApJ, 546, 980
Padoan, P., Jimenez, R., & Jones, B. 1997, MNRAS, 285, 711
Peebles, P. J. E. 1984, ApJ, 277, 470
Peebles, P. J. E., & Dicke, R. H. 1968, ApJ, 154, 891
Press, W. H., & Schechter, P. 1974, ApJ, 187, 425
Pringle, J. E. 1989, MNRAS, 239, 361
Rees, M. J. 1997, Before the Beginning: Our Universe and Others (Reading: Addison-Wesley)
Scalo, J., Vazquez-Semadeni, E., Chappell, D., & Passot, T. 1998, ApJ, 504, 835
Schweizer, F. 1987, in Nearly Normal Galaxies: From the Planck Time to the Present (New York: Springer), 18
Shapley, H. 1930, Star Clusters (New York: McGraw-Hill)
Sheth, R. K., & Tormen, G. 1999, MNRAS, 308, 119
Smith, G. H., Sneden, C., & Kraft, R. P. 2002, AJ, 123, 1502
Sohn, Y., et al. 2003, AJ, 126, 803
Solomon, P. M., Rivolo, A. R., Barrett, J., & Yahil, A. 1987, ApJ, 319, 730
Spergel, D. N., et al. 2003, ApJS, 148, 175
Spitzer, L. 1987, Dynamical Evolution of Globular Clusters (Princeton: Princeton Univ. Press)
van den Bergh, S. 1996, AJ, 112, 2634
———. 2003, ApJ, 590, 797
van Leer, B. 1979, J. Comput. Phys., 32, 101
Vazquez-Semadeni, E. 1994, ApJ, 423, 681
Vázquez-Semadeni, E., Gazol, A., & Scalo, J. 2000, ApJ, 540, 271
Vesperini, E., & Heggie, D. C. 1997, MNRAS, 289, 898
Wada, K., & Norman, C. A. 2001, ApJ, 547, 172
Weil, M. L., & Pudritz, R. E. 2001, ApJ, 556, 164
West, M. J. 1993, MNRAS, 265, 755
Whitmore, B. C. 2000, preprint (astro-ph/0012546)
Whitmore, B. C., & Schweizer, F. 1995, AJ, 109, 960
Whitmore, B. C., Zhang, Q., Leitherer, C., Fall, S. M., Schweizer, F., & Miller, B. W. 1999, AJ, 118, 1551
Wilson, C. D., Scoville, N., Madden, S. C., & Charmandaris, V. 2003, ApJ, 599, 1049
Wong, T., & Blitz, L. 2002, ApJ, 569, 157
Woosley, S. E., & Weaver, T. A. 1995, ApJS, 101, 181
Young, J. S., Allen, L., Kenney, J. D. P., Lesser, A., & Rownd, B. 1996, AJ, 112, 1903
Zepf, S. E., Ashman, K. M., English, J., Freeman, K. C., & Sharples, R. M. 1999, AJ, 118, 752
Zhang, Q., & Fall, S. M. 1999, ApJ, 527, L81
Zhang, Q., Fall, S. M., & Whitmore, B. C. 2001, ApJ, 561, 727